



1 **Spatial-temporal patterns of inorganic nitrogen air concentrations**
2 **and deposition in eastern China**

3 Wen Xu^{1,2}, Lei Liu³, Miaomiao Cheng⁴, Yuanhong Zhao⁵, Lin Zhang⁵, Yuepeng Pan⁶,
4 Xiuming Zhang⁷, Baojing Gu⁷, Yi Li⁸, Xiuying Zhang³, Jianlin Shen⁹, Li Lu¹⁰,
5 Xiaosheng Luo¹¹, Yu Zhao¹², Zhaozhong Feng^{2*}, Jeffrey L. Collett, Jr.¹³, Fusuo
6 Zhang¹, Xuejun Liu^{1*}

7 ¹College of Resources and Environmental Sciences, Key Laboratory of Plant-Soil Interactions of
8 MOE, Beijing Key Laboratory of Cropland Pollution Control and Remediation, China
9 Agricultural University, Beijing 100193, China

10 ²State Key Laboratory of Urban and Regional Ecology, Research Center for Eco-Environmental
11 Sciences, Chinese Academy of Sciences, Shuangqing Road 18, Haidian District, Beijing, 100085,
12 China

13 ³Jiangsu Provincial Key Laboratory of Geographic Information Science and Technology,
14 International Institute for Earth System Science, Nanjing University, Nanjing, 210023, China

15 ⁴State Key Laboratory of Environmental Criteria and Risk Assessment, Chinese Research
16 Academy of Environmental Sciences, Beijing 100012, China

17 ⁵Laboratory for Climate and Ocean-Atmosphere Sciences, Department of Atmospheric and
18 Oceanic Sciences, School of Physics, Peking University, Beijing 100871, China

19 ⁶State Key Laboratory of Atmospheric Boundary Layer Physics and Atmospheric Chemistry
20 (LAPC), Institute of Atmospheric Physics, Chinese Academy of Sciences, Beijing, 100029, China

21 ⁷Department of Land Management, Zhejiang University, Hangzhou 310058, People's Republic of
22 China

23 ⁸Arizona Department of Environmental Quality, Phoenix, AZ 85007, USA

24 ⁹Institute of Subtropical Agriculture, Chinese Academy of Sciences, Changsha 4410125, China

25 ¹⁰Institute of Surface-Earth System Science, Tianjin University, Tianjin, 300072, China

26 ¹¹Institute of Plant Nutrition, Resources and Environmental Sciences, Henan Academy of
27 Agricultural Sciences, Henan Key Laboratory of Agricultural Eco-environment, Zhengzhou,
28 450002, China

29 ¹²State Key Laboratory of Pollution Control & Resource Reuse, School of the Environment,
30 Nanjing University, 163 Xianlin Ave., Nanjing, Jiangsu 210023, China

31 ¹³Department of Atmospheric Science, Colorado State University, Fort Collins, Colorado, 80523
32 USA

33 *Correspondence to: X. J. Liu (liu310@cau.edu.cn) and Z.Z. Feng (fzz@rcees.ac.cn)

34

35

36

37

38

39 **Abstract:**

40 Five-year (2011-2015) measurements of gaseous NH_3 , NO_2 and HNO_3 and particulate
41 NH_4^+ and NO_3^- in air and/or precipitation were conducted at twenty-seven sites in a
42 Nationwide Nitrogen Deposition Monitoring Network (NNDMN) to better understand
43 spatial and temporal (seasonal and annual) characteristics of reactive nitrogen (N_r)
44 concentrations and deposition in eastern China. Our observations reveal annual
45 average concentrations ($16.4\text{--}32.6 \mu\text{g N m}^{-3}$), dry deposition fluxes ($15.8\text{--}31.7 \text{ kg N}$
46 $\text{ha}^{-1} \text{ yr}^{-1}$) and wet/bulk deposition fluxes ($18.4\text{--}28.0 \text{ kg N ha}^{-1} \text{ yr}^{-1}$) based on land use
47 were ranked as urban > rural > background sites. Annual concentrations and dry
48 deposition fluxes of each N_r species in air were comparable at urban and background
49 sites in northern and southern regions, but were significantly higher at northern rural
50 sites. These results, together with good agreement between spatial distributions of
51 NH_3 and NO_2 concentrations determined from ground measurements and satellite
52 observations, demonstrate that atmospheric N_r pollution is heavier in the northern
53 region than in the southern region. No significant inter-annual trends were found in
54 the annual N_r dry and wet/bulk N deposition at almost all of the selected sites. A lack
55 of significant changes in annual averages between the 2013-2015 and 2011-2012
56 periods for all land use types, suggests that any effects of current emission controls
57 are not yet apparent in N_r pollution and deposition in the region. Ambient
58 concentrations of total N_r exhibited a non-significant seasonal variation at all land use
59 types, although significant seasonal variations were found for individual N_r species
60 (e.g., NH_3 , NO_2 and $p\text{NO}_3^-$) in most cases. In contrast, dry deposition of total N_r
61 exhibited a consistent and significant seasonal variation at all land use types, with the
62 highest fluxes in summer and the lowest in winter. Based on sensitivity tests by the
63 GEOS-Chem model, we found that NH_3 emissions from fertilizer use (including
64 chemical and organic fertilizers) were the largest contributor (36%) to total inorganic
65 N_r deposition over eastern China. Our results not only improve the understanding of
66 spatial-temporal variations of N_r concentrations and deposition in this pollution
67 hotspot, but also provide useful information for policy-makers that mitigation of NH_3
68 emissions should be a priority to tackle serious N deposition in eastern China.



69 1. Introduction

70 In China, and globally, human activities have dramatically increased emissions
71 of nitrogen oxides ($\text{NO}_x = \text{NO} + \text{NO}_2$) and ammonia (NH_3) into the atmosphere since the
72 beginning of the industrial revolution (Galloway et al., 2008; Liu et al., 2013). NO_x
73 and NH_3 emitted to the atmosphere are transformed to nitrogen-containing particles
74 (e.g., particulate NH_4^+ and NO_3^- , and organic nitrogen) (Ianniello et al., 2010; Zhang
75 et al., 2015), which are major chemical constituents of airborne $\text{PM}_{2.5}$ (particulate
76 matter with a diameter of 2.5 μm or less) and have implications for air quality and
77 climate (Fuzzi et al., 2015). As a result of elevated N_r emissions, nitrogen (N)
78 deposition through dry and wet processes has also substantially increased over China
79 (Liu et al., 2013; Lu et al., 2007, 2014; Jia et al., 2014, 2016), and excessive
80 deposition of N has resulted in detrimental impacts including decreased biological
81 diversity (Bobbink et al., 2010), nutrient imbalance (Li et al., 2016), increased soil
82 acidification (Yang et al., 2015), eutrophication of water bodies (Fenn et al., 2003),
83 and increased greenhouse gas emissions (Gruber and Galloway, 2008). Furthermore,
84 N_r -associated haze pollution episodes, characterized by high concentrations of $\text{PM}_{2.5}$,
85 occur frequently in China, as evidenced in particular in 2013 (Guo et al., 2014; Huang
86 et al., 2014; Tian et al., 2014).

87 In order to control its notorious air pollution, China has reduced national
88 emissions of SO_2 and particulate matter by 14% and 30%, respectively, from 2005 to
89 2010 (MEPC, 2011). Additionally, stringent measures (e.g., using selective
90 catalytic/non-catalytic reduction systems, and implementing tighter vehicle emission
91 standards) were implemented during the 12th Five Year Plan (FYP) period
92 (2011-2015), with aims to reduce 2015 annual emissions of SO_2 and NO_x by 8% and
93 10%, respectively, relative to 2010 levels (Xia et al., 2016). However, there is as yet
94 no regulation or legislation that deals with national NH_3 emissions and thus emission
95 reductions of SO_2 and NO_x to achieve desired air-quality improvement goals will be
96 compromised (Gu et al., 2014). Significant increases in $\text{PM}_{2.5}$ concentrations have
97 been observed in the years 2013 and 2014 as compared to 2012, excluding the
98 influence of meteorological conditions on inter-annual variations (Liang et al., 2015).



99 Other studies with more conclusive evidence have likewise suggested that NH_3 plays
100 a vital role in sulfate formation and exacerbates severe haze pollution development in
101 urban regions of China (Wang et al., 2016), even acting as the key limiting factor for
102 the formation of secondary inorganic aerosol (Wu et al., 2016). In addition, due to
103 higher local and regional concentrations of NH_3 in the atmosphere, nitrate-driven haze
104 pollution occurred during summertime in urban environment in the North China Plain
105 (Li et al., 2018). The absolute and relative concentrations of particulate nitrate in
106 urban Beijing increased with haze development (Pan et al., 2016). Also, nitrate
107 contributed to a large fraction of the elevated $\text{PM}_{2.5}$ concentrations at a rural site in the
108 North China Plain and high NH_3 in the early morning accelerated the formation of
109 fine nitrates (Wen et al., 2015).

110 High rates of N deposition have also been observed during 2011-2014 across
111 China (Xu et al., 2015). However, to date no study, based on long-term ground-based
112 observations, has provided any information on the effectiveness of SO_2 and NO_x
113 emission controls on N deposition in China. Non-linearities have been identified
114 between reductions in emission and deposition in Europe over the last 3 decades
115 (Aguillaume et al., 2016; Fowler et al., 2007). Due to the tightly coupled yet complex
116 relationship between emissions, concentrations and deposition, long-term monitoring
117 networks can provide a test of the effectiveness of emission controls (Erisman et al.,
118 2003). Currently two national N deposition networks are operational in China, i.e. the
119 Nationwide Nitrogen Deposition Monitoring Network (NNDMN, Liu et al., 2011; Xu
120 et al., 2015) and the Chinese Ecosystem Research Network (CERS, Zhu et al., 2015).
121 The NNDMN containing 43 *in situ* monitoring sites has been operational since 2010
122 to measure wet N deposition and ambient concentrations of five major N_r species (i.e.,
123 gaseous NH_3 , NO_2 and HNO_3 , and particulate NH_4^+ and NO_3^-), the latter for
124 subsequence estimation of dry deposition. The CERS was established in 1988 and
125 mainly focused on wet N deposition at 41 field stations. In addition to ground-based
126 measurements, satellite observations enable retrieval of atmospheric NH_3 and NO_2
127 with high temporal and spatial resolutions (Dammer et al., 2016; Russell et al., 2012),
128 providing a means to reveal spatial distributions and long-term trends of ambient NH_3



129 and NO₂ levels at regional to global scales, and also to evaluate the effectiveness of
130 emission controls (Krotkov et al., 2016). However, to effectively use the vast satellite
131 data sets for environmental monitoring, it is critical to validate these remote sensing
132 observations using *in situ* surface observations (Pinder et al., 2011; Van Damme et al.,
133 2015).

134 Eastern China is a developed region with the largest densities of population,
135 economic activity and resource consumption in the country (He et al., 2015). Recent
136 satellite observations indicate that tropospheric NH₃ and NO₂ levels in eastern China
137 were both much greater than other regions of the world from 2005-2015 (Demmer et
138 al., 2016; Krotkov et al., 2016). Accordingly, this region received the highest levels of
139 dry N deposition in the world (Vet et al., 2014), and was regarded as a primary export
140 region of N deposition for neighboring countries (Ge et al., 2014). Based on
141 meta-analysis of published observations, some studies have provided information on
142 the magnitudes, spatial distributions, and decadal variations of wet/bulk N deposition
143 in China (Liu et al., 2013; Jia et al., 2014), but the analyzed data were limited to time
144 periods between 1980 and 2010. Although a recent study (Jia et al., 2016) has
145 reported a clear increasing trend of dry N deposition in eastern China between 2005
146 and 2014, considerable uncertainty may exist due to estimates of gaseous HNO₃ and
147 particulate NH₄⁺ and NO₃⁻ (*p*NH₄⁺ and *p*NO₃⁻) concentrations using NO₂ satellite data,
148 which is in part manifested by Liu et al. (2017a). Furthermore, seasonal patterns of N_r
149 concentrations and deposition have not yet been systematically investigated at a large
150 spatial scale in this region, although spatial patterns of dry N_r deposition for
151 representative months of four seasons (i.e., January for winter, April for spring, July
152 for summer, October for autumn) in 2010 have been mapped with the RAMS-CMAQ
153 model (Han et al., 2017). Thus, the spatial and temporal (annual and seasonal)
154 variations of N_r concentrations, and dry and wet deposition in eastern China require
155 further exploration using ground-based measurements, especially for time periods
156 after 2010.

157 The present study aims to examine spatial-temporal (annual and seasonal)
158 characteristics of N_r concentrations in air (NH₃, NO₂, HNO₃, *p*NH₄⁺ and *p*NO₃⁻) and



159 precipitation ($\text{NH}_4^+\text{-N}$ and $\text{NO}_3^-\text{-N}$) and their corresponding dry and wet/bulk N
160 deposition, through a 5-year (2011-2015) monitoring period at 27 NNDMN *in situ*
161 sites in eastern China. In addition, we compare spatial-temporal variability of
162 measured NH_3 and NO_2 concentrations with variations of the corresponding satellite
163 retrieval columns, as well as inter-annual trends in N_r deposition and emissions.
164 Finally, emission sources contributing to total N deposition over eastern China are
165 examined.

166 2. Materials and methods

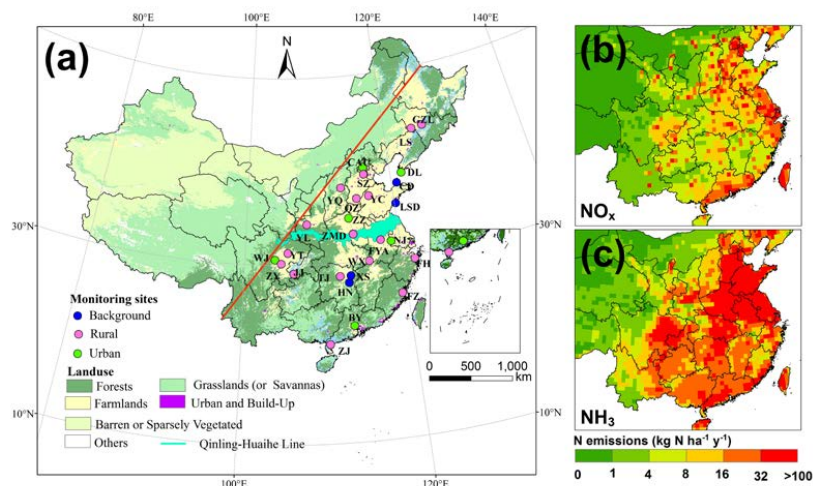
167 2.1 Study area and site descriptions

168 The present study was conducted in eastern China, which is distinguished by the
169 “Hu Line” (She, 1998). This region has spatial heterogeneity in levels of economic
170 development, resulting in significant spatial differences in NH_3 and NO_x emissions
171 (Fig. 1b and c). Thus, to better analyze spatial and temporal variabilities in measured
172 N_r concentrations and deposition, we divided eastern China into northern and southern
173 regions using the Qinling Mountains-Huaihe River line (Fig. 1a), of which the
174 division basin was based on the differences in natural conditions, agricultural
175 production, geographical features and living customs. As for specific differentiations,
176 for example, the northern region adopted a centralized domestic heating policy for
177 late autumn and winter seasons but the south has not; annual average precipitation
178 amounts were generally greater than 800 mm in the south but were less than 800 mm
179 in the north. In addition, the north is characterized by calcareous soil, which could
180 result in higher soil NH_3 volatilization (Huang et al., 2015), vs. the acidic red soil in
181 the south.

182 The NNDMN was operated in line with international standards by China
183 Agricultural University (CAU); 35 NNDMN sites were located in eastern China (Xu
184 et al., 2015). For our analysis, we considered twenty-seven sites in total, with most
185 having continuous data covering 5 years: 13 sites were located north of the Qinling
186 Mountains-Huaihe River line (China Agricultural University-CAU, Zhengzhou-ZZ,
187 Dalian-DL, Shuangzhuang-SZ, Quzhou-QZ, Yangqu-YQ, Zhumadian-ZMD,
188 Yanglin-YL, Yucheng-YC, Gongzhulin-GZL, Lishu-LS, Lingshanda-LSD,



189 Changdao-CD), and 14 sites were located south of the line (Nanjing-NJ, Baiyun-BY,
190 Wenjiang-WJ, Wuxue-WX, Taojing-TJ, Fengyang-FY, Zhanjiang-ZJ, Fuzhou-FZ,
191 Fenghua-FH, Ziyang-ZY, Yangting-YT, Jiangjin-JJ, Huinong-HN, Xishan-XS).



192
193 **Figure 1.** Spatial distributions of the 27 monitoring sites (a), NO_x emissions (b)
194 and NH_3 emissions (c) in Eastern China (NH_3 and NO_x emission data were for the
195 year 2010 and obtained from Liu et al. (2017b)).

196 All the sites are located as far away as possible and practical from local direct
197 emission sources to increase regional representativeness. They can be divided into
198 three categories according to their geopolitical location and their proximity to the
199 main emission sources: urban sites (abbreviated as U), rural sites (cropland areas, R),
200 and background sites (coastal and forest areas, B). Information on the monitoring sites,
201 such as land use types, coordinates, and measurement periods are listed in Table S1 of
202 the Supplement. Detailed descriptions of all the sites including the surrounding
203 environment and nearby emission sources can be found in Xu et al. (2015).

204 2.2 Field sampling and chemical analysis

205 Continuous measurements were performed during the period from January 2011
206 to December 2015 at the 27 study sites, except for eleven sites (ZZ, ZMD, YC, LSD,
207 NJ, WX, FYA, ZJ, YT, JJ, and HN), where field sampling was carried out after the
208 year 2010 and/or interrupted during the period due to instrument failure (details in



209 Table S1, Supplement). Ambient N_r concentrations of gaseous NH_3 and HNO_3 , and
210 pNH_4^+ and pNO_3^- (for which the empirically determined effective size cut-off for
211 aerosol sampling is of the order of $4.5 \mu m$) were measured using an active DELTA
212 (DEnuder for Long-Term Atmospheric sampling; Tang et al., 2009) system; gaseous
213 NO_2 was sampled in three replicates with passive diffusion tubes (Gradko
214 International Limited, UK). The air intakes of the DELTA system and the NO_2 tubes
215 were mounted 2 m above the ground at most sites and protected from precipitation
216 and direct sunlight with a rigid plastic box and a PVC shelter, respectively. All
217 measurements of N_r concentration were based on monthly sampling (one sample per
218 month for each N_r species). Detailed information on measuring methods and
219 collection are given in Sect. S1 of the Supplement.

220 To collect precipitation (here termed as wet/bulk deposition, which contains wet
221 and some dry deposition due to the use of an open sampler) samples, a standard
222 precipitation gauge (SDM6, Tianjin Weather Equipment Inc., China) was
223 continuously exposed beside the DELTA system (ca. 2 m). Immediately after each
224 precipitation event (08:00–08:00 next day, Greenwich Mean Time +8), samples
225 (including rain and melted snow) were collected and stored in clean polyethylene
226 bottles (50 mL) at $-18^\circ C$ until sent to the CAU laboratory for analysis. Each collector
227 was rinsed three times with high-purity water after each collection and once every
228 week to limit contamination from accumulated dust.

229 In the analytical laboratory, acid-coated denuders and aerosol filters were
230 extracted with 6 and 10 mL of high-purity water ($18.2 M\Omega$), respectively, and
231 analyzed for NH_4^+-N with an AA3 continuous-flow analyzer (CFA) (BranC Luebbe
232 GmbH, Norderstedt, Germany). Carbonate-coated denuders and filters were both
233 extracted with 10 mL 0.05% H_2O_2 solution followed by analysis of $NO_3^- -N$ using the
234 same CFA. NO_2 samples, extracted with a solution containing sulfanilamide, H_3PO_4 ,
235 and N-1-naphthylethylene-diamine, were determined using a colorimetric method by
236 absorption at a wavelength of 542 nm (Xu et al., 2016). Precipitation samples were
237 filtered through a syringe filter (0.45 μm , Tengda Inc., Tianjin, China) and analyzed
238 for $NH_4^+ -N$ and $NO_3^- -N$ using the CFA as mentioned above. Quality assurance and



239 quality control procedures adopted in the analytical laboratory are described by Xu et
240 al. (2017). Further details of precipitation measurement, samples handling, and
241 chemical analysis are reported in Xu et al. (2015).

242 **2.3 Deposition estimate**

243 Wet/bulk deposition of $\text{NH}_4^+\text{-N}$ and $\text{NO}_3^-\text{-N}$ were calculated per month and year
244 by multiplying the precipitation amount by their respective volume-weighted mean
245 (VWM) concentrations. The dry deposition flux of gaseous and particulate N_r species
246 was calculated as the product of measured concentrations by modeled deposition
247 velocities (V_d). The dry deposition velocities of five N_r species were calculated by the
248 GEOS (Goddard Earth Observing System)-Chem chemical transport model (CTM)
249 (Bey et al., 2001; <http://geos-chem.org>), and have been reported in a companion paper
250 (Xu et al., 2015). In brief, the model calculation of dry deposition of N_r species
251 follows a standard big-leaf resistance-in-series model as described by Wesely (1989)
252 for gases and Zhang et al. (2001) for aerosol. We used archived hourly V_d from
253 January 2011 to May 2013 and filled the gap for the period (from June 2013 to
254 December 2015) when GEOS meteorological data are unavailable using the mean
255 values calculated from all the available simulations. The monthly V_d at each site was
256 averaged from the hourly dataset.

257 **2.4 Satellite retrievals of NH_3 and NO_2**

258 Comparisons between satellite observations and ground-based measurements
259 were evaluated at the twenty-seven sites in order to accurately examine the
260 spatial-temporal pattern of NH_3 and NO_2 concentrations. For NH_3 , we used the
261 products retrieved from the Infrared Atmospheric Sounding Interferometer (IASI)
262 instrument (aboard the MetOp-A platform), which crosses the equator at a mean local
263 solar time of 9:30 a.m. and 9:30 p.m. The IASI- NH_3 product is based on the
264 calculation of a spectral hyperspectral range index and subsequent conversion to NH_3
265 total columns via a neural network. The details of the IASI- NH_3 retrieval method are
266 described in Whitburn et al. (2016). We only considered the observations from the
267 morning overpass as they are generally more sensitive to NH_3 because of higher
268 thermal contrast at this time of day (Van Damme et al., 2015; Dammers et al., 2016).



269 The daily IASI-NH₃ data (provided by the Atmospheric Spectroscopy Group at
270 Université Libre De Bruxelles, data available at [http://iasi.aeris-data.fr/NH₃/](http://iasi.aeris-data.fr/NH3/)) from 1
271 January 2011 to 31 December 2015 was used in the present study. We did not use the
272 IASI_NH₃ after 30 September 2014 for the temporal analysis because an update of the
273 input meteorological data had caused a substantial increase in the retrieved
274 atmospheric NH₃ columns. Only observations with a cloud coverage lower than 25%,
275 and relative error lower than 100% or absolute error smaller than 5×10^{15} molecules
276 cm⁻² were processed. The methodology is provided in detail in Liu et al. (2017b). In
277 brief, all observations were gridded to a 0.5° latitude × 0.5° longitude grid, and then
278 we calculated the monthly arithmetic mean by averaging the daily values with
279 observations points within each grid cell. Similarly, we calculated the annual
280 arithmetic mean by averaging the daily values with observations points within the grid
281 cell over the whole year.

282 For NO₂ we used the products from the Ozone Monitoring Instrument (OMI)
283 resided on NASA's EOS-Aura satellite, which was launched in July 2004 into a
284 sun-synchronous orbit with a local equator crossing time at approximately 1:45 p.m.
285 OMI detects the backscattered solar radiation from the Earth's atmosphere within the
286 UV-vis spectral window between 270-500 nm, to achieve nearly global coverage daily,
287 with a spatial resolution ranging from 13 km × 24 km at nadir to 24 km × 128 km at
288 the edge of the swath (Russell et al., 2012). We used tropospheric NO₂ retrievals from
289 the DOMINO (Dutch Finnish Ozone Monitoring Instrument) algorithm version 2. The
290 retrieval algorithm is described in detail in Boersma et al. (2007). The tropospheric
291 NO₂ columns used in this study are monthly means from 1 January 2011 to 30
292 December 2015 with a spatial resolution of 0.125° latitude × 0.125° longitude (data
293 available at <http://www.temis.nl/airpollution/no2.html>).

294 2.5 Statistical analysis

295 One-way analysis of variance (ANOVA) and two-independent-samples *t* tests
296 were applied to detect significant differences in seasonal mean concentrations and
297 deposition fluxes of measured N_r species as well as their annual mean deposition
298 fluxes for three land use types (rural, urban and background). As there was large



299 site-to-site variability in annual N_r concentrations and deposition fluxes at monitoring
300 sites within the same land use types, averaging data into annual values for land use
301 types is unlikely to be truly representative of actual trends. Thus, annual trends of the
302 variables were evaluated at a single site scale rather than by land use type. Trend
303 analysis was conducted using Theil regression (Theil, 1992) and the Mann-Kendall
304 test (Gilbert, 1987; Marchetto et al., 2013). We defined an increasing (decreasing)
305 trend as a positive (negative) slope of the Theil regression, while a statistical
306 significance level ($p < 0.01$) of a trend was evaluated by the non-parametric
307 Mann-Kendall test (p value). Non-parametric methods usually have the advantage of
308 being insensitive to outliers, and allow missing data and non-normal distribution of
309 data (Gilbert, 1987; Salmi et al., 2002), appropriate for the analyzed data set. The
310 Mann-Kendall method is appropriate for detection of monotonic trends in data series
311 that have no seasonal variation or autocorrelation. Atmospheric concentrations and
312 deposition fluxes of N_r species, however, generally have distinct seasonal variability
313 (Pan et al., 2012) and the Mann-Kendall test is thus applied to annual values.

314 Satellite observations during 2005-2015 indicate that tropospheric NO_2 levels
315 peaked in 2011 over China (Krotkov et al., 2016; Duncan et al., 2016) and NO_x
316 emissions peaked in 2011/2012 (Miyazaki et al., 2017; van der A et al., 2017; Souri et
317 al., 2017). To assess the impact of emission control measures on measured N_r
318 concentrations and deposition fluxes at different land use types, we compared
319 arithmetic mean values averaged from the last 3-year period (2013-2015) with those
320 averaged from the first 2-year period (2011-2012) for monitoring sites with
321 continuous 5-year measurements (22 sites for dry, and 17 sites for wet/bulk). Seasonal
322 concentrations and deposition fluxes of measured N_r species were calculated using the
323 arithmetic average of matched seasons during the sampling periods; spring refers to
324 March-May, summer covers June-August, autumn refers to September-November,
325 and winter covers December-February.

326

327

328



329 3. Results

330 3.1 Spatial variability in concentrations of N_r species in air and precipitation

331 Summary statistics of monthly mean concentrations of NH_3 , NO_2 , HNO_3 , pNH_4^+ ,
 332 and pNO_3^- at the twenty-seven monitoring sites during 2011-2015 are listed in Table
 333 S2 of the Supplement. Monthly mean concentrations of NH_3 , NO_2 , HNO_3 , pNH_4^+ , and
 334 pNO_3^- ranged from 0.16 (TJ)-39.57 (WJ), 0.55 (LS)-29.06 (WJ), 0.04 (YQ)-4.93
 335 (CAU), 0.11 (ZY)-57.20 (QZ), and 0.01 (DL)-32.06 (ZZ) $\mu g N m^{-3}$, respectively. On
 336 the basis of geographical location and classification of each site, the annual mean
 337 concentrations of each N_r species were calculated for three land use types in eastern
 338 China and its northern and southern regions (Table 1).

339 **Table 1.** Annual average (standard error) concentrations of various N_r compounds in
 340 air and precipitation at different land use types in eastern China and its northern and
 341 southern regions for the 5-year period 2011-2015.

Region ^a	LUY ^b	Ambient conc. $\mu g N m^{-3}$						Rainwater conc. $mg N L^{-1}$		
		NH_3	NO_2	HNO_3	pNH_4^+	pNO_3^-	Total N_r	NH_4^+	NO_3^-	TIN
EC	Urban	8.5	10.2	1.6	8.2	4.0	32.6	1.6	1.9	3.5
	(n=6)	(1.4)	(1.0)	(0.2)	(1.8)	(0.8)	(4.1)	(0.3)	(0.2)	(0.5)
	Rural	7.2	6.0	1.2	6.7	2.8	23.9	1.7	1.4	3.1
	(n=17)	(0.9)	(0.5)	(0.1)	(1.1)	(0.3)	(2.7)	(0.2)	(0.2)	(0.4)
	BKD ^c	3.9	5.2	0.9	4.5	1.9	16.4	1.4	1.2	2.6
	(n=4)	(0.6)	(0.3)	(0.1)	(0.4)	(0.3)	(1.4)	(0.3)	(0.4)	(0.6)
NREC	Urban	8.1	11.7	1.6	8.6	5.1	35.1	2.2	2.4	4.6
	(n=3)	(2.4)	(1.6)	(0.3)	(2.3)	(1.4)	(7.7)	(0.4)	(0.2)	(0.4)
	Rural	9.9	7.4	1.4	9.2	3.7	31.6	2.4	2.0	4.4
	(n=8)	(1.2)**	(0.7)*	(0.1)*	(1.9)*	(0.5)*	(3.8)**	(0.3)**	(0.2)**	(0.4)**
	BKD	4.7	5.7	1.0	5.1	2.4	18.8	1.8	1.5	3.3
	(n=2)	(0.6)	(0.3)	(0.1)	(0.2)	(0.3)	(0.1)	(0.2)	(0.3)	(0.1)
SREC	Urban	8.9	8.7	1.6	7.9	2.9	30.1	1.1	1.5	2.6
	(n=3)	(1.8)	(0.6)	(0.1)	(3.1)	(0.2)	(4.5)	(0.3)	(0.3)	(0.6)
	Rural	4.9	4.6	1.0	4.5	1.9	17.0	1.1	0.9	2.0
	(n=9)	(0.6)	(0.6)	(0.1)	(0.6)	(0.2)	(1.7)	(0.2)	(0.1)	(0.3)
	BKD	3.1	4.7	0.8	4.0	1.4	14.0	1.0	0.6	1.6
	(n=2)	(0.7)	(0.4)	(0.1)	(0.2)	(0.2)	(0.6)	(0.0)	(0.0)	(0.0)

342 ^aEC: eastern China; NREC: northern region of eastern China; SREC: southern region



343 of eastern China. ^b LSY: land use type; n denotes number of monitoring sites. ^c BKD:
344 Background. *Significant at the 0.05 probability level. **Significant at the 0.01
345 probability level.

346 In eastern China, annual mean concentrations of NH₃, NO₂, HNO₃, pNH₄⁺, and
347 pNO₃⁻ at the urban sites (1.6 ± 0.2 to 10.2 ± 1.0 μg N m⁻³) were 18-44% and 78-120%
348 higher than their corresponding concentrations at the rural (1.2 ± 1.0 to 7.2 ± 0.9 μg N
349 m⁻³) and background (0.9 ± 0.1 to 5.2 ± 0.3 μg N m⁻³) sites, respectively. Analogous
350 patterns also occurred for all measured N_r in each region, except for NH₃ and pNH₄⁺
351 in the northern region, for which the mean concentrations were 18% and 7% lower at
352 the urban sites than at the rural sites, respectively.

353 Comparing northern vs. southern regions (Table 1), at urban sites the annual
354 mean concentrations of NH₃, HNO₃, and pNH₄⁺ showed smaller non-significant
355 differences (-1~9%), whereas NO₂ and pNO₃⁻ showed larger non-significant increases
356 (34 and 76%, respectively) in the north. By contrast, the mean concentrations of all
357 measured N_r species were significantly (*p*<0.05) higher (by 40-104%) at rural sites in
358 northern region. Similarly, individual concentrations at background sites were 21-71%
359 higher in the northern than southern region. The annual concentrations of total N_r (i.e.,
360 the sum of five N_r species) decreased in the order urban > rural > background in
361 eastern China as a whole and in the north and south regions; further, the annual total
362 N_r concentrations at urban and background sites were 17 and 34% higher (*p*>0.05) in
363 the north than in the south, respectively, whereas those at northern rural sites (31.6 ±
364 3.8 μg N m⁻³) were significantly (*p*<0.05) higher than the mean at southern rural sites
365 (17.0 ± 1.7 μg N m⁻³).

366 The monthly VWM concentrations of NH₄⁺-N, NO₃⁻-N, and TIN (the sum of
367 NH₄⁺-N and NO₃⁻-N) were in the ranges 0.01 (BY)-26.77 (YC), 0.06 (XS)-28.92 (WJ),
368 and 0.09 (XS)-50.29 (YC) mg N L⁻¹, respectively (Table S3, Supplement). In eastern
369 China and in each region, the annual VWM concentrations of NO₃⁻-N and TIN
370 showed a declining trend of urban > rural > background, whereas those of NH₄⁺-N
371 followed the order rural ≥ urban > background (Table 1). Comparing northern and
372 southern regions, the annual concentrations of NH₄⁺-N, NO₃⁻-N, and TIN were

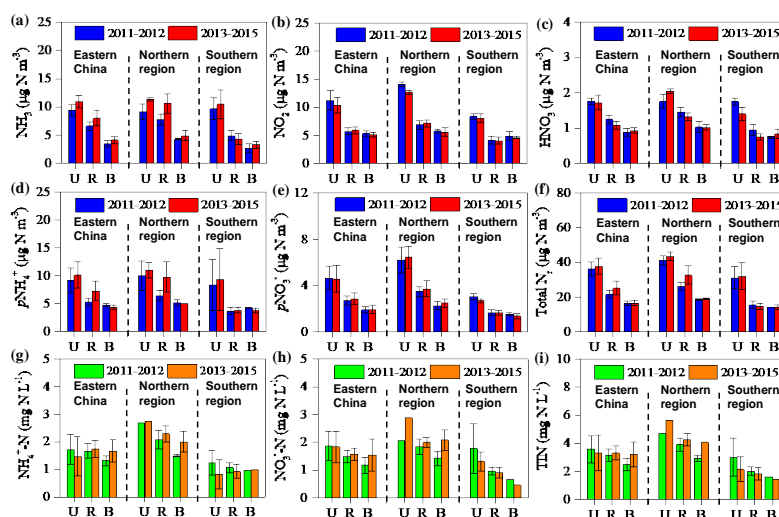


373 comparable at urban and background sites, and were significantly ($p < 0.05$) higher at
374 northern rural sites.

375 **3.2 Annual variability in concentrations of N_r species in air and precipitation**

376 During the 2011-2015 period the annual mean concentrations of measured N_r
377 species in air exhibited no significant trends at the twenty-two selected sites except
378 for NH_3 at four sites (ZZ, DL, ZMD, YL), HNO_3 at three sites (DL, LSD, BY),
379 pNH_4^+ at one site (XS), and total N_r at three sites (ZMD, YL, WJ) (Fig. S1a-f,
380 Supplement). Similarly, no significant trends were found for the annual VWM
381 concentrations of NH_4^+-N , $NO_3^- -N$, and TIN in precipitation at the seventeen selected
382 sites, with the exception of $NO_3^- -N$ at one site (SZ) (Fig. S2a-c, Supplement).

383 Fig. 2 compares annual average concentrations of all measured N_r species
384 between the periods 2013-2015 and 2011-2012 for three land use types. In eastern
385 China the mean concentrations of NH_3 and pNH_4^+ showed non-significant increases
386 (10-38%) at all land use types except pNH_4^+ at background sites, which showed a
387 small reduction (8%) (Fig. 2a, d). By contrast, the mean concentrations of remaining
388 N_r species at three land use types showed smaller and non-significant changes: -8-3%
389 for NO_2 (Fig. 2b), -13-5% for HNO_3 (Fig. 2c), and -1-5% for pNO_3^- (Fig. 2e). The
390 relative changes in the annual total N_r concentration were also not significant, with the
391 largest increase at rural sites (16%) and smaller increases at urban (4%) and
392 background (1%) sites (Fig. 2f). Separated by regions, annual mean concentrations of
393 five N_r species at three land use types mostly showed increases (4-57%) in the north,
394 and reductions (0.3-21%) in the south (Fig. 2a-f). The relative changes in individual
395 concentrations at northern rural sites (9% reduction for HNO_3 , and 9-52% increases
396 for the other species) and southern rural sites (4% increase for pNH_4^+ , and 0.3-21%
397 reductions for other species) were not significant. The annual total N_r concentrations
398 showed small relative changes (from -1% to 5%) across all land use types in the two
399 regions, except at northern rural sites, which exhibited a larger but non-significant
400 increase (25%) (Fig. 2f). Due to significant interannual variability, longer records are
401 needed to better assess the significance of any concentration changes.



402

403 **Figure 2.** Comparison of annual mean concentrations of (a) NH_3 ; (b) NO_2 ; (c) HNO_3 ;
 404 (d) $p\text{NH}_4^+$; (e) $p\text{NO}_3^-$; and (f) total N_r : sum of all measured N_r in air and
 405 volume-weighted concentrations of NH_4^+ (g); NO_3^- (h) and total inorganic N (TIN):
 406 sum of NH_4^+ and NO_3^- (i) in precipitation between the 2011-2012 period and the
 407 2013-2015 period for different land use types in eastern China and its northern and
 408 southern regions. The number of sites for each land use type in each region can be
 409 found in Table S1 in the Supplement. The error bars are the standard errors of means.

410

411 In eastern China, the annual VWM concentrations of $\text{NH}_4^+\text{-N}$, $\text{NO}_3^-\text{-N}$ and TIN
 412 showed the largest increase of 26-31% at background sites, a smaller increase of 4-5%
 413 at rural sites, and a decrease of 2-14% at urban sites; however, those changes were not
 414 significant (Fig. 2g-i). Regionally, their respective concentrations showed increases
 415 (3-45%) in the north and reductions (5-33%) in the south, except for a small increase
 416 (4%) in $\text{NH}_4^+\text{-N}$ at background sites.

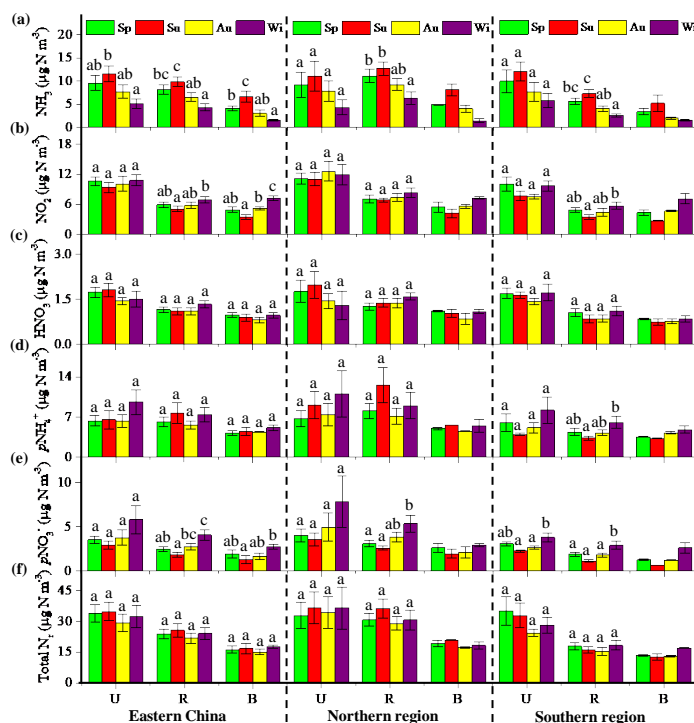
417 3.3 Seasonal variability in concentrations of N_r species in air and precipitation

418 Fig. 3 shows seasonal patterns of NH_3 , NO_2 , HNO_3 , $p\text{NH}_4^+$, $p\text{NO}_3^-$ and total N_r ;
 419 concentrations for three land use types in eastern China and its northern and southern
 420 regions, averaged from corresponding measurements at the twenty-seven study sites
 421 (details for each site are given in Tables S4-S9 of the Supplement). Average NH_3



422 concentrations at all land use types decreased in the order summer > spring > autumn >
 423 winter, and significant seasonal differences generally occurred between summer and
 424 winter (Fig. 3a). Conversely, the average NO₂ concentration generally showed the
 425 highest value in winter and the lowest in summer; differences between seasonal
 426 concentrations were sometimes significant at rural sites in the south and background
 427 sites, but not at urban sites (Fig. 3b). The seasonal changes in the HNO₃ concentration
 428 were generally small and not significant for all land use types (Fig. 3c).

429 The average pNH₄⁺ concentration exhibited a non-significant seasonal variation
 430 across all land use types, except for southern rural sites which showed significantly
 431 higher values in winter than in summer (Fig. 3d). The highest pNH₄⁺ concentrations
 432 mostly occurred in winter. The average pNO₃⁻ concentrations at all land use types
 433 followed the order winter > spring, ~ autumn > summer; the seasonal changes are
 434 sometimes significant, except for urban sites in eastern China and its northern region
 435 (Fig. 3e). The average concentration of total N_r usually showed small and
 436 non-significant seasonal differences for all land use types (Fig. 3f).

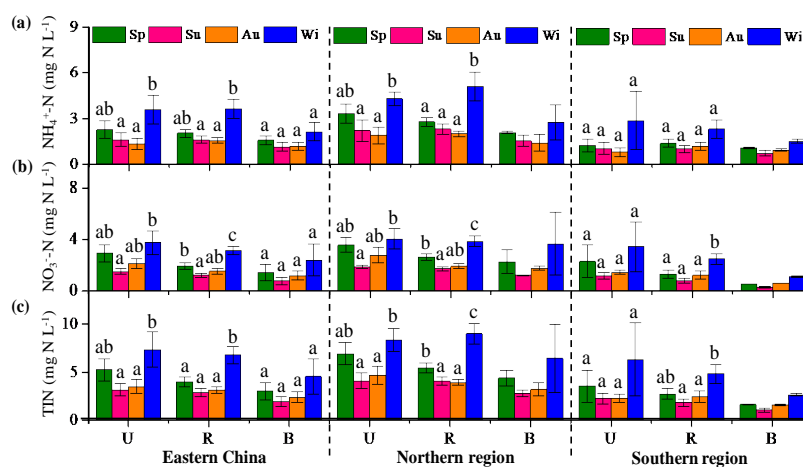


437



438 **Figure 3.** Seasonal mean concentrations of (a) NH_3 ; (b) NO_2 ; (c) HNO_3 ; (d) $p\text{NH}_4^+$;
439 (e) $p\text{NO}_3^-$; and (f) total N_r : sum of all measured N_r in air at different land use types in
440 eastern China and its northern and southern regions. Sp, Su, Au, and Wi represent
441 spring, summer, autumn, and winter, respectively. The number of sites for each land
442 use type in each region can be found in Table S1 in the Supplement. The error bars are
443 the standard errors of means, and different letters on the bars denote significant
444 differences between the sites ($p < 0.05$).

446 In eastern China and its two regions, the seasonal VWM concentrations of
447 $\text{NH}_4^+\text{-N}$, $\text{NO}_3^-\text{-N}$ and TIN in precipitation at three land use types (averaged from the
448 twenty-seven sites, details in Tables S10-S12 of the Supplement) showed a similar
449 seasonal pattern, with the highest values in winter and the lowest in summer or autumn (Fig. 4a-c). Significant seasonal differences usually occurred between winter
450 and the other three seasons at all land use types, except background sites and southern
451 urban sites.
452 urban sites.



453
454 **Figure 4.** Seasonal mean concentrations of NH_4^+ (a); NO_3^- (b) and total
455 inorganic N (TIN): sum of NH_4^+ and NO_3^- (c) in precipitation at different land use
456 types in eastern China and its northern and southern regions. Sp, Su, Au, and Wi
457 represent spring, summer, autumn, and winter, respectively. The number of sites for
458 each land use type in each region can be found in Table S1 in the Supplement. The



459 error bars are the standard errors of means, and different letters on the bars denote
460 significant differences between the sites ($p < 0.05$).

461 **3.4 Spatial variability in dry and wet/bulk N deposition of N_r species**

462 Dry deposition fluxes of NH_3 , HNO_3 , NO_2 , pNH_4^+ , and pNO_3^- ranked in the
463 order urban > rural > background in eastern China and in both southern and northern
464 regions (except for pNH_4^+ in the north) (Table 2). Comparing northern and southern
465 regions, at urban sites the mean dry pNH_4^+ deposition was slightly higher (2%) in the
466 north, whereas larger enhancements (24-69%) in the mean fluxes were found in the
467 north for the remaining N_r species. By contrast, individual fluxes were significantly
468 higher (by 64-138%) at northern rural sites, except for HNO_3 which showed a large
469 non-significant increase (58%). At northern background sites, the mean dry deposition
470 fluxes of NH_3 and NO_2 were much higher (159%) and lower (68%), respectively;
471 however, only small differences in the means were found for HNO_3 (6% lower in the
472 north), pNH_4^+ (5% lower), and pNO_3^- (14% higher). The spatial pattern of total N dry
473 deposition flux (the sum of the fluxes of the five N_r species) by land use types ranked
474 in the same order as individual N_r species in eastern China. Compared with the
475 southern region, mean total N fluxes in the north region were significantly higher (by
476 85%) at rural sites, but showed non-significant increases at urban and background
477 sites (33 and 38%, respectively).

478 The wet/bulk deposition fluxes of NH_4^+-N , $NO_3^- -N$, and TIN ranked in the order
479 urban > rural > background in eastern China and in each region (except for NH_4^+-N in
480 the south) (Table 2). In addition, their respective fluxes were generally comparable in
481 northern and southern regions.

482
483
484
485
486
487
488



489 **Table 2.** Annual average (standard error) dry and wet/bulk deposition fluxes (kg N
 490 $\text{ha}^{-1} \text{yr}^{-1}$) of various N_r compounds at different land use types in eastern China and its
 491 northern and southern regions for the 5-year period 2011-2015.

Region ^a	LUY ^b	Dry deposition					Wet/bulk deposition			
		NH_3	NO_2	HNO_3	$p\text{NH}_4^+$	$p\text{NO}_3^-$	Total N_r	NH_4^+	NO_3^-	TIN
EC	Urban	12.6	4.4	7.7	4.8	2.1	31.7	12.6	15.4	28.0
	(n=6)	(1.4)	(1.2)	(1.6)	(1.4)	(0.5)	(4.6)	(1.9)	(0.7)	(2.2)
	Rural	9.1	2.9	4.6	4.0	1.5	22.1	11.9	10.2	22.1
	(n=17)	(0.9)	(0.3)	(0.6)	(0.7)	(0.2)	(2.3)	(1.0)	(0.5)	(1.4)
	BKD ^c	7.9	1.8	3.5	1.9	0.8	15.8	10.7	7.7	18.4
	(n=4)	(2.1)	(0.6)	(0.2)	(0.3)	(0.1)	(1.5)	(1.8)	(0.3)	(1.8)
NREC	Urban	13.9	5.2	9.4	4.9	2.7	36.2	13.9	14.1	28.0
	(n=3)	(1.9)	(2.5)	(3.0)	(1.9)	(1.0)	(8.2)	(3.5)	(1.0)	(4.4)
	Rural	12.1 ^{**}	3.6 [*]	5.7	5.7 [*]	2.1 ^{**}	29.3 ^{**}	12.3	10.3	22.6
	(n=8)	(1.3)	(0.4)	(1.0)	(1.2)	(0.3)	(3.2)	(1.3)	(0.7)	(1.8)
	BKD	11.4	0.9	3.4	1.9	0.8	18.4	7.8	7.6	15.4
	(n=2)	(0.6)	(0.7)	(0.3)	(0.7)	(0.2)	(0.7)	(1.4)	(0.8)	(0.6)
SREC	Urban	11.2	3.6	5.9	4.8	1.6	27.2	11.4	16.6	28.0
	(n=3)	(2.0)	(0.3)	(0.6)	(2.6)	(0.2)	(4.0)	(2.0)	(0.4)	(2.1)
	Rural	6.5	2.2	3.6	2.4	1.0	15.8	11.6	10.2	21.8
	(n=9)	(0.5)	(0.4)	(0.6)	(0.4)	(0.2)	(1.4)	(1.5)	(0.9)	(2.2)
	BKD	4.4	2.7	3.6	2.0	0.7	13.3	13.6	7.9	21.5
	(n=2)	(1.0)	(0.2)	(0.3)	(0.1)	(0.1)	(0.7)	(0.1)	(0.1)	(0.1)

492 ^aEC: eastern China; NREC: northern region of eastern China; SREC: southern region
 493 of eastern China. ^bLSY: land use type; n denotes number of monitoring sites. ^c BKD:
 494 Background. ^{*}Significant at the 0.05 probability level. ^{**}Significant at the 0.01
 495 probability level.

496 3.5 Annual variability in dry and wet/bulk N deposition

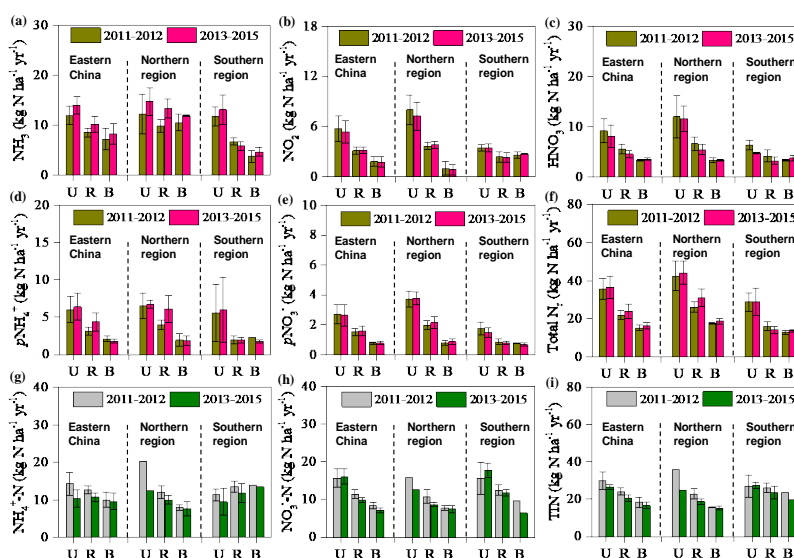
497 The annual trends of dry deposition fluxes of individual N_r species at the
 498 twenty-two selected sites are consistent with trends in their respective ambient
 499 concentrations, except for HNO_3 at three sites (SZ, LSD, and ZY) (Figs. S3a-e and
 500 S1a-e, Supplement). A consistent picture is also seen for the total dry N deposition
 501 fluxes at all but two sites (DL and WJ) (Figs. S3f and S1f, Supplement). Similarly, the
 502 annual trends of wet/bulk deposition fluxes of NH_4^+ -N, NO_3^- -N and TIN at seventeen
 503 selected sites are similar to their respective concentrations in precipitation (Fig. S4a-c,



504 Supplement).

505 In eastern China the annual average dry deposition fluxes of NH_3 , NO_2 , HNO_3 ,
 506 $p\text{NH}_4^+$ and $p\text{NO}_3^-$ showed non-significant increases (2-39%) or reductions (1-19%)
 507 between the periods 2011-2012 and 2013-2015 at the three land use types (Fig. 5a-e),
 508 similar in sign and magnitude to their respective concentrations described earlier. The
 509 annual average total N dry deposition fluxes showed small and non-significant
 510 increases across the study periods: 2% at urban sites, 9% at rural sites, and 7% at
 511 background sites (Fig. 5f). The sign and magnitude of period-to-period changes in dry
 512 deposition and ambient concentrations of all measured N_r species were generally
 513 similar between the southern and northern regions.

514 Wet/bulk deposition fluxes of NH_4^+ -N, NO_3^- -N, and TIN generally decreased
 515 (4-29%) between 2011-2012 and 2013-2015 periods at all land use types in eastern
 516 China; one exception was NO_3^- -N, which exhibited a small increase (3%) at urban
 517 sites (Fig. 5g-i). Similar tendencies were also observed in both northern and southern
 518 regions.



519

520 **Figure 5.** Comparison of dry deposition of (a) NH_3 ; (b) NO_2 ; (c) HNO_3 ; (d) $p\text{NH}_4^+$;
 521 (e) $p\text{NO}_3^-$; and (f) total N_r : sum of all measured N_r in air and wet/bulk deposition of
 522 NH_4^+ (g); NO_3^- (h) and total inorganic N (TIN): sum of NH_4^+ and NO_3^- (i) in



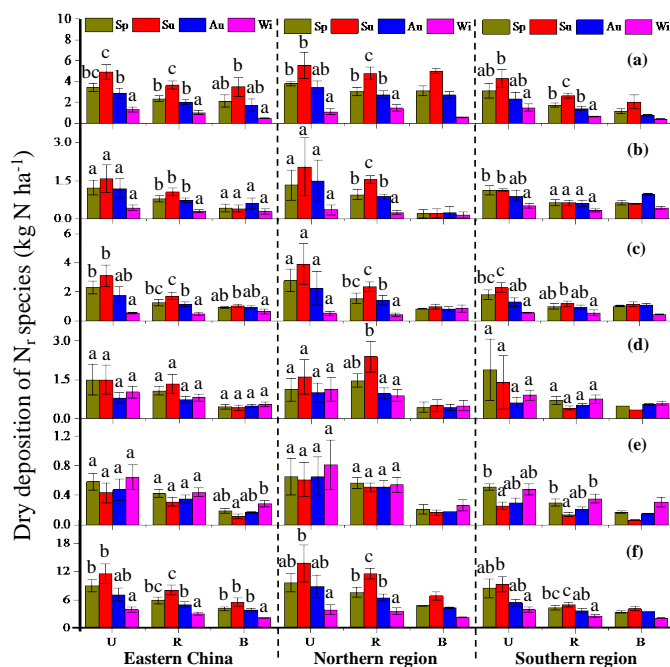
523 precipitation between the 2011-2012 period and the 2013-2015 period for different
 524 land use types in eastern China and its northern and southern regions. The number of
 525 sites for each land use type in each region can be found in Table S1 in the Supplement.

526 The error bars are the standard errors of means.

527

528 3.6 Seasonal variability in dry and wet/bulk deposition of N_r species

529 Seasonal variations of dry deposition of individual N_r species at each site are
 530 shown in Tables S4-S9 in the Supplement. In eastern China and in each region, dry
 531 NH_3 deposition fluxes at all land use types followed the order summer > spring >
 532 autumn > winter, with the seasonal changes usually significantly different (Fig. 6a).
 533 Similarly, dry the NO_2 deposition flux was also at its minimum in winter, but its
 534 maximum was found in summer at urban and rural sites and in autumn at background
 535 site; seasonal differences in most cases were not significant (Fig. 6b). Seasonal
 536 patterns of dry HNO_3 deposition flux at all land use types were similar to those for dry
 537 NH_3 deposition fluxes, and the resulting seasonal changes were sometimes significant,
 538 except at northern urban sites (Fig. 6c).



539

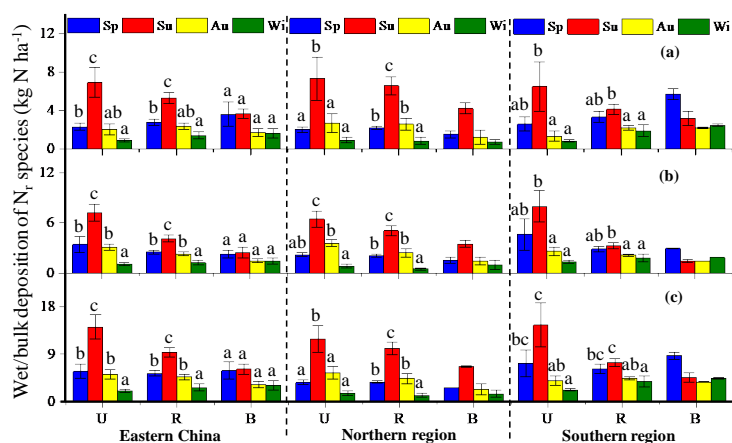


540 **Figure 6.** Seasonal mean dry deposition of (a) NH_3 ; (b) NO_2 ; (c) HNO_3 ; (d) $p\text{NH}_4^+$;
541 (e) $p\text{NO}_3^-$; and (f) total N_r : sum of all measured N_r in air at different land use types in
542 eastern China and its northern and southern regions. Sp, Su, Au, and Wi represent
543 spring, summer, autumn, and winter, respectively. The number of sites for each land
544 use type in each region can be found in Table S1 in the Supplement. The error bars are
545 the standard errors of means, and different letters on the bars denote significant
546 differences between the sites ($p < 0.05$).

547

548 Dry $p\text{NH}_4^+$ deposition fluxes peaked in spring or summer at urban and rural sites,
549 but remained at similar levels across the four seasons at background sites; however,
550 no significant seasonal variations were found at any land use types except for rural
551 sites in the north (Fig. 6d). Dry $p\text{NO}_3^-$ deposition fluxes were higher in spring and
552 winter than in summer and autumn at all land use types, and the seasonal changes
553 were sometimes significant at background sites and at southern urban and rural sites
554 (Fig. 6e). Total dry N deposition fluxes at all land use types showed similar seasonal
555 variations to dry NH_3 deposition, with the highest values in summer and the lowest in
556 winter; significant seasonal differences generally were observed between winter and
557 the other three seasons (Fig. 6f).

558 Wet/bulk deposition fluxes of $\text{NH}_4^+\text{-N}$, $\text{NO}_3^-\text{-N}$, and TIN all showed significant
559 seasonal variation at urban and rural sites, but not at background sites, with the
560 highest values in summer and the lowest in winter (Fig. 7a-c).



561

562

563

564

565

566

567

568

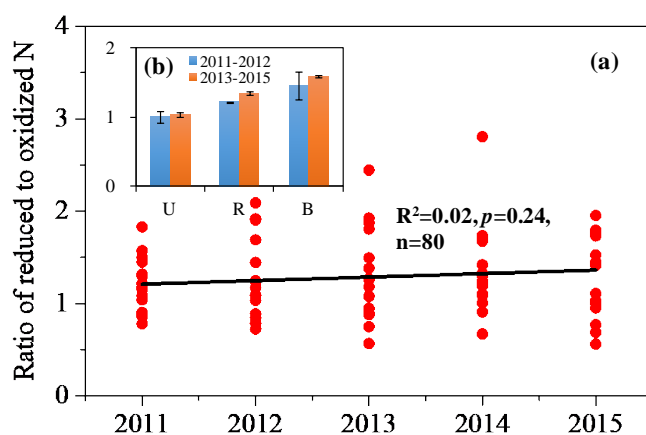
569

570 **3.7 Spatial-temporal variability in total annual dry and wet/bulk deposition of N_i**
 571 **species**

572 In eastern China total annual mean N deposition (dry plus wet/bulk) fluxes at
 573 rural and background sites were comparable (on average, 44.3 ± 3.0 and 34.3 ± 0.7 kg
 574 $N\ ha^{-1}\ yr^{-1}$, respectively), but significantly lower than those at urban sites (59.7 ± 6.1
 575 $kg\ N\ ha^{-1}\ yr^{-1}$) (Tables 1 and 2, and Fig. S5, Supplement). Similar tendencies for total
 576 N deposition fluxes were observed in the southern region, while in the north a
 577 significant difference was only found between urban and background sites (Fig. S5,
 578 Supplement). From 2011 to 2015, no significant annual trend was found in the total N
 579 deposition at sixteen selected sites (Fig. S6a, Supplement). The total annual mean N
 580 deposition fluxes at three land use types showed small and non-significant reductions
 581 (1-5%) between 2011-12 and 2013-15 (Fig. S6b, Supplement). Regionally, the total



582 fluxes at each land use type were of similar magnitude in the two periods. Also, the
583 NH_x (wet/bulk NH_4^+ -N deposition plus dry deposition of NH_3 and particulate
584 NH_4^+)/ NO_y (wet/bulk NO_3^- -N deposition plus dry deposition of NO_2 , HNO_3 and
585 particulate NO_3^-) ratio showed a non-significant annual trend across all sites (**Fig. 8a**).
586 At all land use types, the averaged ratios were slightly higher in the 2013-2015 period
587 than in the 2011-2012 period (Fig. 8b).



588
589 **Figure 8.** Annual trend of the ratio of NH_x (wet/bulk NH_4^+ -N deposition plus dry
590 deposition of NH_3 and particulate NH_4^+) to NO_y (wet/bulk NO_3^- -N deposition plus dry
591 deposition of NO_2 , HNO_3 and particulate NO_3^-) across sixteen selected sites (**a**), with
592 a comparison between the 2011-2012 period and the 2013-2015 period for different
593 land use types in eastern China (**b**). The number of sites with the same land use type
594 can be found in Fig. S6 in the Supplement.

595

596 4. Discussion

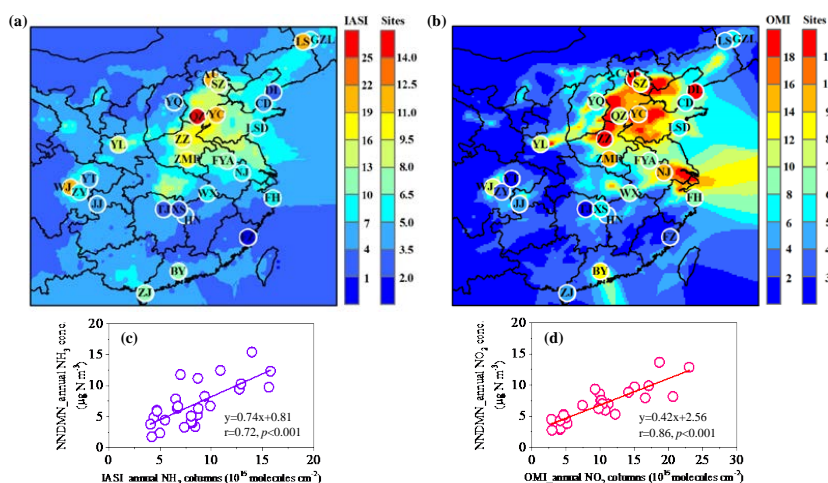
597 4.1 Comparisons of NH_3 and NO_2 measurements with satellite data

598 Eastern China, as a highly industrialized and polluted region and has been
599 proven to be a hot spot of N_r (NH_3 and NO_x) emission and deposition globally (Vet et
600 al., 2014; Kanakidou et al., 2016). The results presented above showed that, in eastern
601 China, annual mean concentrations of measured N_r species in air and precipitation
602 were generally higher in the north than in the south (Table 1). This is likely due to



603 higher consumption of energy and application of N-fertilizers, along with lower
604 precipitation amounts in the north, previously identified as key factors affecting
605 spatial patterns of N deposition in China (Jia et al., 2014; Zhu et al., 2015). Because
606 only 27 sites covering a range of land use types were included in the present study,
607 additional information would be valuable in determining whether the observed spatial
608 patterns adequately represent conditions in eastern China. To address this issue, we
609 use measured NH₃ and NO₂ concentrations to evaluate remote sensing techniques for
610 retrieving NH₃ and NO₂ concentrations. If accurate, those remote sensing techniques
611 are well suited to ascertain regional species distributions. NH₃ and NO_x are primary
612 emissions with important anthropogenic emissions (Fowler et al., 2013). NO, the
613 main component of emitted NO_x, is oxidized in the atmosphere to NO₂. NO₂ is further
614 oxidized via daytime or nighttime chemistry to HNO₃ (Khoder, 2002). NH₃ and
615 HNO₃ can react to form fine particle ammonium nitrate (Seinfeld and Pandis, 2006).
616 Thus, spatial patterns of NH₃ and NO₂ observed from space can be useful indicators
617 of reduced and oxidized N_r pollution over eastern China.

618 From satellite observations (Fig. 9a, b), it can be seen that both IASI_NH₃ and
619 OMI_NO₂ columns show clearly higher values over the northern region of eastern
620 China. Overall, satellite observations and surface measurements for NH₃ and NO₂
621 (plotted on the maps of Fig. 9a, b) show a similar spatial pattern. Significant positive
622 correlations were found between IASI_NH₃ column observations and NNDMN_NH₃
623 measurements ($r=0.72$, $p<0.001$) (Fig. 9c) and between OMI_NO₂ observations and
624 NNDMN_NO₂ measurements ($r=0.86$, $p<0.001$) (Fig. 9d) at the 27 surface
625 measurement locations, suggesting that satellite measurements of NH₃ and NO₂ can
626 be used to capture regional differences in NH₃ and NO₂ pollution. Looking beyond
627 the surface measurement location, the satellite observations further confirm the
628 existence of greater N_r pollution in the northern region of eastern China than in the
629 southern region.



630

631

632

633

634

635

636

637

638

639

640

641

642

643

644

645

646

647

648

649

650

Figure 9. Spatial variation of atmospheric N_r in eastern China: **(a)** NNDMN_ NH_3 concentrations vs. IASI_ NH_3 columns; **(b)** NNDMN_ NO_2 concentrations vs. OMI_ NO_2 columns; **(c)** relationship of NNDMN_ NH_3 concentrations vs. IASI_ NH_3 columns; **(d)** relationship of NNDMN_ NO_2 concentrations vs. OMI_ NO_2 columns.

To further explore temporal concentration variability, monthly mean satellite NH_3 and NO_2 columns are compared with monthly mean ground concentrations of NH_3 and NO_2 (Figs. S7 and S8, Supplement). The linear correlation between satellite columns and surface NH_3 concentrations is significant ($p < 0.05$) at the ten sites ($r = 0.32$ – 0.87) in the northern region and at four sites ($r = 0.46$ – 0.84) in the southern region (Fig. S7, Supplement), while the linear correlation between satellite columns and surface NO_2 concentrations is significant at the ten sites ($r = 0.28$ – 0.68) in the northern region and nine sites ($r = 0.36$ – 0.66) in the southern region (Fig. S8, Supplement). These results indicate that the OMI_ NO_2 retrieval can well capture the temporal variations of surface NO_2 concentrations over eastern China, whereas the IASI_ NH_3 retrievals better capture temporal variability in surface concentrations for the northern region. The weak correlations observed between IASI_ NH_3 observations and surface measurements at ten of the fourteen sites in the southern region (Fig. S7, Supplement) suggest that the IASI_ NH_3 observations need to be improved for investigating temporal variability in NH_3 concentration, despite that the satellite



651 observation is at a specific time of day while the surface concentrations integrate
652 across the diurnal cycle of emissions and mixing layer evolution. It should be noted
653 that a direct comparison between surface concentration and satellite column
654 measurements is inevitably affected by many factors, such as changes in boundary
655 layer height, vertical profiles of species, and interferences from cloud and aerosol
656 (Van Damme et al., 2015). Nevertheless, the ratio of satellite column to surface
657 concentration measurements is meaningful as it can provide insight into sensitivity of
658 a satellite retrieval to variation in the concentration of a gas in the surface layer (Meng
659 et al., 2008). To make a more accurate comparison, the vertical profile is
660 recommended to convert the columns to the ground concentrations in future work.

661 **4.2 Seasonal variations of N_r concentration and deposition**

662 The seasonal concentrations of N_r species in air and precipitation are dependent
663 on their sources and meteorological conditions. The highest concentrations of NH_3 in
664 summer at all land use types (Fig. 3a) are most likely due to enhanced NH_3 emission
665 from natural and fertilized soils, and biological sources such as humans, sewage
666 systems and organic waste in garbage containers (Chang et al., 2016). Zhang et al.
667 (2018) showed that NH_3 emissions in China show a strong summer peak, with
668 emissions about 50% higher in summer than spring and autumn. The lowest
669 concentrations of NH_3 in winter (Fig. 3a) can be ascribed to the reduced NH_3
670 volatilization at low air temperature, high snow coverage, and low agricultural
671 activities (Cao et al., 2009) as well as consumption of NH_3 to form NH_4NO_3 (Fig. 3a,
672 d and e) and/or $(NH_4)_2SO_4$. The lower NO_2 concentration in summer (Fig. 3b) might
673 result from greater atmospheric mixing in a deeper boundary layer and a higher rate of
674 oxidation of NO_2 to HNO_3 by reaction with OH (Atkins and Lee, 1995), which is
675 more abundant in summer due to greater photochemical activity. Increased NO_2
676 emissions from greater coal combustion for domestic heating (from middle November
677 to middle March) in Northern China may also enhance NO_x emissions and subsequent
678 NO_2 concentrations in autumn/winter (Zhao et al., 2011).

679 Nitric acid is a secondary pollutant, formed through gas phase reaction of NO_2
680 with the OH radical, reaction of NO_3 with aldehydes or hydrocarbons or hydrolysis of



681 N_2O_5 (Khoder, 2002). Nitric acid concentrations are expected to be further influenced
682 by air temperature, relative humidity and ambient NH_3 concentrations (Allen et al.,
683 1989); fine particle NH_4NO_3 formation is favored at low temperatures and high
684 relative humidities. Due to a lack of information regarding primary formation
685 pathways and influencing factors at our study sites, we cannot offer a definitive
686 explanation for small and differing seasonal patterns of HNO_3 concentrations
687 observed at the three land use types (Fig. 3c). Particulate NH_4^+ and NO_3^- are also
688 mainly generated via chemical reactions between NH_3 and inorganic acids (e.g.,
689 HNO_3 , H_2SO_4). We found that concentrations of $p\text{NH}_4^+$ and $p\text{NO}_3^-$ at all land use
690 types usually peaked in winter (Fig. 3e, f). Low temperature and high emissions of
691 NO_x and SO_2 in winter are favorable for formation of ammonium sulfate ($(\text{NH}_4)_2\text{SO}_4$)
692 and ammonium nitrate (NH_4NO_3) aerosols (Xu et al., 2016), consistent with higher
693 concentrations of $p\text{NH}_4^+$ and $p\text{NO}_3^-$. In addition, in winter temperature inversions in
694 combination with stable meteorological conditions (e.g., low wind speed) limit
695 horizontal and vertical exchange of pollutants, and further elevated atmospheric
696 $p\text{NH}_4^+$ and $p\text{NO}_3^-$ levels (Liu et al., 2017).

697 Ammonium-N and nitrate-N in precipitation mainly originate from
698 corresponding reduced (e.g., NH_3 , $p\text{NH}_4^+$) and oxidized (e.g., HNO_3 , NO_2 , $p\text{NO}_3^-$) N
699 in air, scavenged respectively, by rain and/or snow events (Seinfeld and Pandis, 2006).
700 At all land use types, the seasonal variation of NH_4^+ -N concentration in precipitation
701 was opposite to that of reduced N (the sum of NH_3 and $p\text{NH}_4^+$) concentrations (Figs.
702 4a and S9a in the Supplement), whereas a similar seasonal pattern was found between
703 NO_3^- -N and oxidized N (the sum of HNO_3 , NO_2 and $p\text{NO}_3^-$) concentrations (Figs. 4b
704 and S9b in the Supplement). Higher precipitation amounts in summer could account
705 for lower NH_4^+ -N concentrations in summer (Figs. 4a and S10 in the Supplement) due
706 to a dilution effect (Xu et al., 2015). In contrast, seasonal variations of rainwater
707 NO_3^- -N concentrations were more likely dominated by seasonal changes in oxidized
708 N concentrations rather than precipitation amount.

709 The seasonal variation of NH_3 dry deposition is generally similar to that of NH_3
710 concentration (Figs. 3a and 6a). Given comparable seasonal mean V_d for NH_3 across



711 the four seasons in most cases (Fig. S11a-c, Supplement), the seasonality of NH_3
712 deposition is mainly dominated by changes in ambient NH_3 concentrations. Seasonal
713 deposition fluxes of NO_2 and HNO_3 both differ appreciably (Fig. 6b, c), showing
714 similar variation to seasonality of their respective V_d values (Fig. S11d-i, Supplement).
715 Given weaker seasonal fluctuations of NO_2 and HNO_3 concentrations, the seasonality
716 of NO_2 and HNO_3 dry deposition are primarily functions of changes in V_d . Similar
717 analyses suggest that seasonal variation of $p\text{NO}_3^-$ dry deposition was mainly caused
718 by differences in seasonal $p\text{NO}_3^-$ concentrations (Figs. 3e and 6e), whereas that of
719 $p\text{NH}_4^+$ dry deposition was primarily driven by seasonal changes in V_d (Figs. 6c and
720 S11j-l, Supplement).

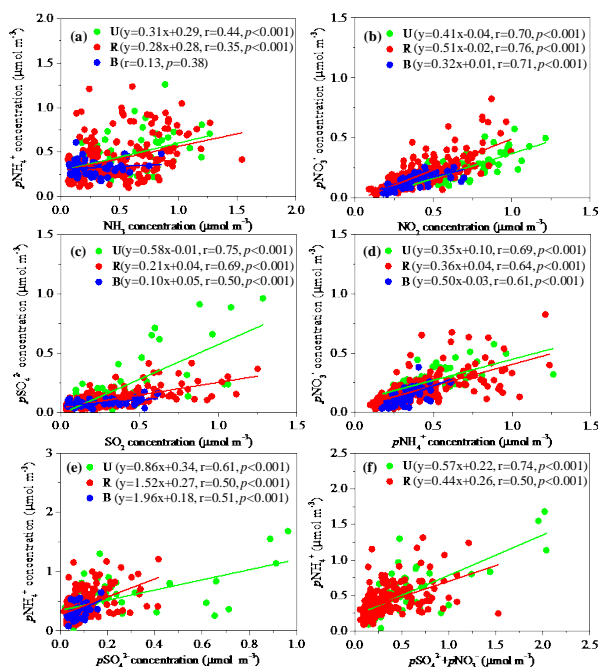
721 4.3 The role of NH_3 in mitigation of N_r air pollution

722 The latest pollutant emissions statistics from the Chinese Ministry of
723 Environmental Protection
724 (http://www.zhb.gov.cn/gkml/hbb/qt/201507/t20150722_307020.htm) showed that
725 total annual emissions of SO_2 and NO_x were reduced by 12.9% and 8.6% in 2014,
726 respectively, compared with those in 2010. This suggests that the goal set for the 12th
727 FYP period was fulfilled ahead of time. Our field measurements demonstrate that
728 annual mean concentrations of each N_r species and total N_r did not show significant
729 decreasing trends at most sites during the 2011-2015 period (Fig. S1a-f, Supplement).
730 Furthermore, annual mean total N_r concentrations showed non-significant increases
731 (1-16%) at three land use types during the 2013-2015 period compared with
732 2011-2012 (Fig. 2f). These results together suggest that N_r pollution may be not
733 effectively mitigated in eastern China during the 12th FYP, likely due to the absence of
734 NH_3 regulations, despite enforcement of a “Zero Increase Action Plan” by the
735 Ministry of Agriculture for national fertilizer use (X. J. Liu et al., 2016).

736 Ammonia is the primary alkaline gas in the atmosphere. It plays an important
737 role in formation of $(\text{NH}_4)_2\text{SO}_4$ and NH_4NO_3 aerosols (Seinfeld and Pandis, 2006).
738 These secondary inorganic aerosols account for 40–57 % of the $\text{PM}_{2.5}$ concentrations
739 in eastern China (Yang et al., 2011; Huang et al., 2014). Based on monthly mean
740 molar concentrations, there were significant positive linear correlations between NH_3



741 and $p\text{NH}_4^+$, NO_2 and $p\text{NO}_3^-$, SO_2 and $p\text{SO}_4^{2-}$, $p\text{NH}_4^+$ and $p\text{NO}_3^-$, and $p\text{NH}_4^+$ and
 742 $p\text{SO}_4^{2-}$ at all land use land types except for a non-significant relationship of NH_3 with
 743 $p\text{NH}_4^+$ at background sites (Fig. 10a-e). These results suggest that the precursor gases
 744 are responsible for the formation of secondary inorganic ions (i.e., $p\text{NH}_4^+$, $p\text{NO}_3^-$, and
 745 $p\text{SO}_4^{2-}$) locally at urban and rural sites, while secondary inorganic ions at background
 746 sites likely originated from long-distance transport. The ratio of NH_3 to NH_x (NH_3
 747 plus $p\text{NH}_4^+$) concentrations at urban (0.53 ± 0.15) and rural (0.52 ± 0.16) sites
 748 exceeded values at background (0.43 ± 0.16) sites. According to Walker et al. (2004),
 749 a value greater than 0.5 indicates that NH_x is more likely to be from local sources as
 750 opposed to long-range transport.



751
 752 **Figure 10.** Correlations of monthly mean molar concentrations of (a) $p\text{NH}_4^+$ vs. NH_3 ;
 753 (b) $p\text{NO}_3^-$ vs. NO_2 ; (c) $p\text{SO}_4^{2-}$ vs. SO_2 ; (d) $p\text{NO}_3^-$ vs. $p\text{NH}_4^+$; (e) $p\text{NH}_4^+$ vs. $p\text{SO}_4^{2-}$; (f)
 754 $p\text{NH}_4^+$ vs. $(p\text{SO}_4^{2-} + p\text{NO}_3^-)$ at three land use types in eastern China. The number of
 755 sites with the same land use type in each region can be found in Table S1 in the
 756 Supplement.

757 It is known that NH_3 in the atmosphere is preferentially neutralized by H_2SO_4 to



758 form $(\text{NH}_4)_2\text{SO}_4$ and/or NH_4HSO_4 , with any remainder available for potential reaction
759 with HNO_3 to form NH_4NO_3 . At urban and rural sites, monthly mean $p\text{NH}_4^+$
760 concentrations significantly positively correlated with the sum of $p\text{SO}_4^{2-}$ and $p\text{NO}_3^-$
761 concentrations (Fig. 10f). However, the slopes of regression equations between them
762 were both smaller than unity (0.57 and 0.44 at urban and rural sites, respectively),
763 indicating an incomplete neutralization of acidic species (HNO_3 and H_2SO_4) by NH_3
764 at urban and rural sites. In other words, NH_3 is a factor limiting the formation of
765 secondary inorganic ions. A model simulation by Wang et al. (2011) found that,
766 without NH_3 emission controls, NO_3^- in $\text{PM}_{2.5}$ will be enhanced by 10% in 2030
767 compared with 2005 in China, despite improved NO_x emissions controls. As reported
768 by Zhang et al. (2017), total NH_3 emissions in China increased from $12.1 \text{ Tg N yr}^{-1}$ in
769 2000 to $15.6 \text{ Tg N yr}^{-1}$ in 2015 at an annual rate of 1.9%. In contrast, total emissions
770 of NO_x and SO_2 have decreased or stabilized in recent years, and were estimated to be
771 8.4 Tg N yr^{-1} and $12.5 \text{ Tg S yr}^{-1}$ in 2014, respectively (Xia et al., 2016). Based on
772 these factors, implementation of NH_3 control strategies, relative to current NO_x and
773 SO_2 emission controls, should be considered to mitigate atmospheric N_r pollution.

774 4.4 The role of NH_3 emission in control of N deposition

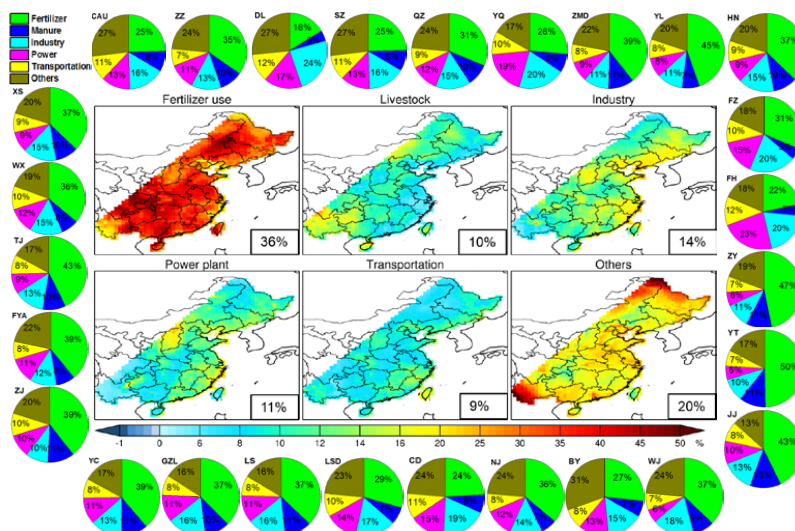
775 The present results showed that total dry N deposition fluxes at three land use
776 types were higher in the northern region of eastern China than in the southern region
777 (Table 1), mainly due to higher NH_3 dry deposition resulting from higher NH_3
778 concentrations in the north. This is especially true for northern rural sites (Table 1),
779 mostly located in the North China Plain (NCP) (see details in Xu et al. (2015)). The
780 NCP (that is, Beijing and Tianjin cities and Hebei, Henan, and Shandong provinces), a
781 highly populated region with intensive agricultural production, contributes 30-40% of
782 the total annual NH_3 emissions in China (Huang et al., 2012). Thus, we anticipate that
783 reducing NH_3 emissions can effectively control N deposition.

784 To further examine contributions of NH_3 emissions to total (wet plus dry) N
785 deposition at each site and over eastern China, we conducted model sensitivity tests
786 using the nested GEOS-Chem atmospheric chemistry model driven by the GEOS-5
787 assimilated meteorological fields at a horizontal resolution of $1/2^\circ \times 2/3^\circ$. The model



788 used anthropogenic emissions from the Multi-Resolution Emission Inventory of
789 China (MEIC, <http://meicmodel.org>) for the year 2010, except for NH₃ emissions that
790 are taken from the Regional Emission in Asia (REAS-v2) inventory (Kurokawa et al.,
791 2013), with an improved seasonality derived by Zhao et al. (2015). In brief,
792 anthropogenic sources of NH₃ emissions include fertilizer use, livestock, human waste,
793 and fuel combustion (that in power plant, industry, transportation and residential),
794 whereas NO_x emission sources include industry, power, transportation, and residential.
795 Both NH₃ and NO_x have natural sources (including lightning, biomass burning and soil
796 emissions). It should be pointed out that fertilizer NH₃ emissions include both
797 chemical fertilizer and manure fertilizer. Details of the model emissions and
798 mechanisms have been described elsewhere (Zhao et al., 2017, Xu et al., 2018).

799 We evaluate the model simulations by comparing with measured bulk (both
800 NH₄⁺-N and NO₃⁻-N) fluxes. The model biases for bulk NH₄⁺-N and NO₃⁻-N
801 deposition were 23 and -23%, respectively (Fig. S8, Supplement). These biases are
802 reasonable, given uncertainties in N_r emissions and predictions of meteorology. Given
803 that model evaluation is not central to this work, we presented the details in Sect. S1
804 in the Supplement. As shown in Fig. 11, fertilizer use is the dominant source of total
805 N deposition at all sites, with contributions between 16-50%. Also, over eastern China
806 the largest contribution was from fertilizer use (36%) relative to livestock (10%),
807 industry (14%), power plant (11%), transportation (9%), and other sources (20%, the
808 sum of contributions from human waste, residential activities, soil, lighting and
809 biomass burning). These results indicate that reducing NH₃ emissions from improper
810 fertilizer (including chemical and organic fertilizer) application should be a priority in
811 curbing N deposition in eastern China.



812

813 **Figure 11.** Fractional contributions to total N deposition from emission sectors (i.e.
814 fertilizer use, livestock, industry, power plant, transportation, and others including
815 emissions from human waste, residential activities, soil, lighting and biomass burning)
816 at the twenty-seven sites and over eastern China.

817

818 4.5 Deposition response to emission change

819 Similar to N_r concentrations, there were no significant decreasing trends in dry
820 and bulk deposition of total N or of individual N_r species at almost all study sites
821 (Figs. S3 and S4, Supplement). In addition, we found that changes in annual mean
822 deposition fluxes of various N_r species are fairly small between the 2013-2015 and
823 2011-2012 periods (Fig. 5). These results suggest that current emission controls did
824 not effectively reduce N deposition in eastern China.

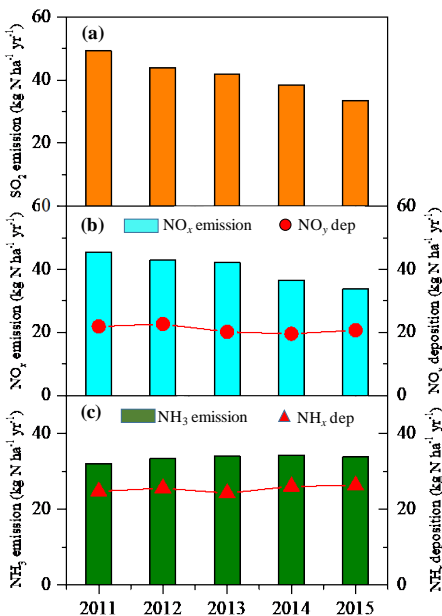
825 To further assess the relationship between emission and deposition change, we
826 considered the emissions of SO_2 , NO_x and NH_3 affecting the sixteen study sites with
827 continuous and simultaneous dry and bulk deposition measurements (Fig. S6 and
828 Table S1, Supplement). The regional NH_3 emission data for 2011-2015 were derived
829 from Zhang et al. (2017), while SO_2 and NO_x emission data for 2011-2014 were
830 derived from Xia et al. (2016) (emission data for the year 2015 were provided by Prof.
831 Yu Zhao, and were unpublished). We compared these annual data with annual mean



832 deposition values from the 16 sites. It should be noted that such assessment is subject
833 to some uncertainty, as emission data was estimated based on the areas belonging to
834 eastern China.

835 A clear decreasing trend in SO_2 and NO_x emissions was observed, with
836 reductions of 32% and 25% in 2015 compared to 2011, respectively (Fig. 12a, b). This
837 reduction is directly related to the widespread use of selective catalytic reduction and
838 flue gas de-sulfurization on power plants and industries (Van der A et al., 2017), and
839 to a lesser extent to the introduction of new emission standards for cars (F. Liu et al.,
840 2016). In contrast, NH_3 emissions generally showed a gradual increasing trend
841 between 2011 and 2015 (Fig. 12c), as control strategies have not yet been enacted and
842 implemented for NH_3 emissions in China.

843



844

845 **Figure 12.** Emission of SO_2 (a), NO_x (b) and NH_3 (c) obtained as average data from
846 the areas belonging to eastern China, compared with deposition values in the same
847 periods (mean values from the sixteen sites showing in Fig. S6 and Table S1 in the
848 Supplement, 5-year averages).

849 Regarding N deposition, a non-significant increasing trend was found for NH_x



850 (slope=0.36 kg N ha⁻¹ yr⁻¹) between the 2011 and 2015 period, whereas NO_y
851 deposition exhibited a non-significant decreasing trend (slope=0.54 kg N ha⁻¹ yr⁻¹).
852 Also, there were non-significant linear correlations between NH_x deposition and NH₃
853 emission and between NO_y deposition and NO_x emission. This is not surprising given
854 that atmospheric chemistry is complex and often behaves non-linearly (Fowler et al.,
855 2007; Fagerli and Aas, 2008). Interactions between the different pollutants,
856 precipitation variability, changes in the relative amounts and lifetimes of the chemical
857 species and in gas-particle partitioning all may contribute to the lack of correlation
858 between emission and deposition trends. Non-linearities between emission and
859 deposition change have been described also elsewhere (Aguillaume et al., 2016;
860 Karlsson et al., 2011). Deposition in eastern China is also influenced by emissions
861 from outside the region, further degrading any expected correlation with local
862 emissions.

863 **4.6 Uncertainties and limitations**

864 The present study examined annual trends of concentrations of N_r species in air
865 and precipitation as well as dry and bulk N deposition based on Kendall tests and only
866 five annual data values (2011-2015). Although the test can use as few as 4 data points,
867 indications of statistically significant trends for datasets are unlikely to be truly
868 representative of the trends that are actually occurring due to in the short duration of
869 the measurement dataset. Longer time series (e.g., more than 10-year) will likely
870 allow detection of more significant time trends in future work. Another uncertainty
871 may arise from the fact that we used fixed monthly mean dry deposition velocities of
872 gaseous and particulate N_r species for the same months from June 2013 to December
873 2015. Nevertheless, the uncertainty in the V_d value did not largely affect the
874 deposition trend, as the annual trend in dry deposition of N_r species is more likely
875 driven by changes in ambient N_r concentrations than to changing deposition velocities,
876 as evident from fairly low standard deviations of annual mean V_d of N_r species at our
877 selected 27 sites between 2008 and 2012 (~0.029 for NH₃, ~0.005 for NO₂, ~0.054 for
878 HNO₃, and ~0.019 for both pNH₄⁺ and pNO₃⁻, data were extracted from Zhao et al.
879 (2017)).



880 In addition, we did not account for inter-annual changes in meteorology, which
881 also strongly influences atmospheric N_r levels and N deposition (Xu et al., 2015,
882 2017). For example, air concentrations of NO_2 , NH_3 , and pNH_4^+ and pNO_3^- trend to
883 increase under the relatively stagnant conditions prior to a cold front's arrival and
884 decrease substantially after the cold front brings precipitation and strong winds into
885 the region (Xu et al., 2017). On the inter-annual time scale, the frequency of cold front
886 passages may be affected by large-scale circulation patterns such as the position of the
887 Siberian high for eastern China (Jia et al., 2015). Given that *in-situ* measurements of
888 meteorological variables are not available, and that GEOS-5 assimilated
889 meteorological fields were updated after May 2013, an evaluation of the effect of
890 meteorology on N_r concentration and deposition is recommended for future work.

891 Uncertainties also exist in the source attribution calculated with the GEOS-Chem
892 simulations, since results largely depend on the emission inventories fed to the model.
893 Zhao et al. (2017) pointed out that uncertainties in current NH_3 emissions inventories
894 (e.g. large range of the emission value in current studies and absence of inclusion of
895 bi-directional NH_3 exchange between the land and atmosphere) may influence
896 nitrogen deposition simulation in China. Future work based on improved NH_3
897 emission inventories (e.g., Zhang et al., 2018) and including bidirectional ammonia
898 exchange with the surface is essential to better examine source attribution of N
899 deposition in China.

900 5. Conclusion

901 We have characterized spatial and temporal (annual and seasonal) variations in
902 concentrations and deposition of major N_r species in air (NH_3 , NO_2 , HNO_3 , pNH_4^+ ,
903 and pNO_3^-) and precipitation (NH_4^+ -N and NO_3^- -N) for three land use types (e.g.,
904 urban, rural and background) in eastern China by examining five-year (2011-2015) *in*
905 *situ* measurements at twenty-seven sites. We further examined regional features of N_r
906 pollution by comparison of satellite and surface measurements of NH_3 and NO_2 and
907 examined the sources of total N deposition over the whole region for the year 2010
908 using the GEOS-Chem model at horizontal resolution of $1/2^\circ \times 2/3^\circ$. Our major
909 results and conclusions are as follows:



910 In eastern China, annual mean concentrations and dry and bulk deposition fluxes
911 of measured N_r species in air and precipitation generally ranked in the order urban >
912 rural > background. The air concentrations and dry deposition were usually higher at
913 all land use types in the northern region of eastern China than in the southern region,
914 especially (except HNO_3) at rural sites, for which the differences reached statistically
915 significant levels. This is also true for the annual VWM concentrations of NH_4^+-N ,
916 NO_3^--N , and TIN in precipitation, whereas bulk deposition fluxes of these species
917 were comparable for matched land use types between the northern and southern
918 regions.

919 No significant trends in the annual mean concentrations and dry and bulk
920 deposition fluxes of measured N_r species in air and precipitation were observed at
921 almost all sites during the 2011-2015 period. Also, annual averages of these values
922 showed non-significant changes between the 2011-2012 and 2013-2015 periods for all
923 land use types. Ambient total concentrations of measured N_r species showed a
924 non-significant seasonal variation at all land use types, whereas individual N_r species
925 exhibited a significant seasonal variation in most cases, except for NO_2 and pNH_4^+ at
926 urban sites, and HNO_3 at all land use types. Unlike air concentrations, dry deposition
927 of total N_r showed a consistent and significant seasonal variation for each land use
928 type, with the highest values in summer and the lowest values in winter. The V_d was a
929 dominant factor influencing seasonal variations of NO_2 , HNO_3 , and pNH_4^+
930 concentrations, while seasonal variations of NH_3 and pNO_3^- are mainly influenced by
931 their respective air concentrations. The concentrations of NH_4^+-N , NO_3^--N , and TIN in
932 precipitation showed significant seasonal variations, ranking in a consistent order of
933 winter > spring > autumn ~ summer. Also, significant seasonal variations in bulk
934 deposition were also found, following in a consistent order of summer > spring ~
935 autumn > winter.

936 Both IASI satellite-retrieved NH_3 columns and OMI satellite-retrieved NO_2
937 columns over eastern China showed higher values in the north than in the south. In
938 addition, significant positive correlations were found between measured NH_3
939 concentrations and retrieved NH_3 columns, and between measured NO_2



940 concentrations and columns. These results together reveal that atmospheric N_r
941 pollution is more serious in the northern region, and also suggest that satellite
942 retrievals of NH_3 and NO_2 columns can provide useful information on spatial
943 concentration variability of these two key N_r species at a regional or national scale.
944 Weak correlations between IASI_ NH_3 observations and surface NH_3 measurements
945 were found at most selected sites, suggesting that IASI_ NH_3 observations in their
946 current state are not as readily used to accurately track temporal variability in surface
947 NH_3 concentrations.

948 Ammonia is currently not included in China's emission control policies of air
949 pollution precursors, although the necessity of mitigation has been the subject of
950 discussion during recent years. Across all urban and rural sites, the slopes of the
951 regression relation between pNH_4^+ and the sum of pSO_4^{2-} and pNO_3^- were both
952 smaller than unity, indicating control of NH_3 emission not only can directly reduce
953 ambient NH_3 concentrations, but also lower the formation of pNH_4^+ and pNO_3^- .
954 Fertilizer use contributed 36% of the total N deposition over eastern China,
955 suggesting reducing NH_3 emissions from fertilizer application would be an effective
956 strategy for reducing N deposition. Overall, our findings reveal persistent serious N_r
957 pollution during the 12th FYP period despite implementation of current emission
958 controls, and highlight the importance of NH_3 emission control on mitigating future
959 atmospheric N_r concentrations and deposition in eastern China.

960

961 **Acknowledgments**

962 This study was supported by the National Key R&D Program of China
963 (2017YFC0210101 & 2017YFC0210106, 2014BC954202), the National Natural
964 Science Foundation of China (41705130, 41425007, 31421092) as well as the
965 National Ten-thousand Talents Program of China (X.J. Liu).

966

967

968

969



970 **References**

- 971 Aguilhaume, L., Rodrigo, A., Avila, A.: Long-term effects of changing atmospheric
972 pollution on throughfall, bulk deposition and streamwaters in a Mediterranean
973 forest, *Sci. Total Environ.* 544, 919–928,
974 <https://doi.org/10.1016/j.scitotenv.2015.12.017>, 2016.
- 975 Allen, A. G., Harrison, R. M., and Erisman, J. W.: Field measurements of the
976 dissociation of ammonium nitrate and ammonium chloride aerosols, *Atmos.*
977 *Environ.*, 23, 1591–1599, 1989.
- 978 Atkins, D. H. F., and Lee, D. S.: Spatial and temporal variation of rural nitrogen
979 dioxide concentrations across the United Kingdom, *Atmos. Environ.*, 29, 223–239,
980 1995.
- 981 Bobbink, R., Hicks, K., Galloway, J., Spranger, T., Alkemade, R., Ashmore, M.,
982 Bustamante, M., Cinderby, S., Davidson, E., and Dentener, F.: Global assessment
983 of nitrogen deposition effects on terrestrial plant diversity: a synthesis, *Ecol. Appl.*
984 20, 30–59, 2010.
- 985 Boersma, K. F., Eskes, H. J., Veefkind, J. P., Brinksma, E. J., van der A, R. J., Sneep,
986 M., van den Oord, G. H. J., Levelt, P. F., Stammes, P., Gleason, J. F., and Bucsela,
987 E. J.: Near-real time retrieval of tropospheric NO₂ from OMI, *Atmos. Chem.*
988 *Phys.*, 7, 2103–2118, <https://doi.org/10.5194/acp-7-2103-2007>, 2007.
- 989 Cao, J. J., Zhang, T., Chow, J. C., Watson, J. G., Wu, F., and Li, H.: Characterization
990 of atmospheric ammonia over Xi'an, China, *Aerosol Air Qual. Res.*, 9, 277–289,
991 2009.
- 992 Chang, Y. H., Liu, X. J., Deng, C. R., Dore, A. J., and Zhuang, G. S.: Source
993 apportionment of atmospheric ammonia before, during, and after the 2014 APEC
994 summit in Beijing using stable nitrogen isotope signatures, *Atmos. Chem. Phys.*, 16,
995 11635–11647, <https://doi.org/10.5194/acp-16-11635-2016>, 2016.
- 996 Dammers, E., Palm, M., Van Damme, M., Vigouroux, C., Smale, D., Conway, S.,
997 Toon, G. C., Jones, N., Nussbaumer, E., Warneke, T., Petri, C., Clarisse, L.,
998 Clerbaux, C., Hermans, C., Lutsch, E., Strong, K., Hannigan, J. W., Nakajima, H.,
999 Morino, I., Herrera, B., Stremme, W., Grutter, M., Schaap, M., Wichink Kruit, R. J.,



- 1000 Notholt, J., Coheur, P. F., and Erisman, J. W.: An evaluation of IASI-NH₃ with
1001 ground-based Fourier transform infrared spectroscopy measurements, Atmos.
1002 Chem. Phys., 16, 10351–10368, <https://doi.org/10.5194/acp-16-10351-2016>, 2016.
- 1003 Erisman, J.W., Grennfelt, P., and Sutton, M.: The European perspective on nitrogen
1004 emission and deposition. Environ. Int., 29, 311–325,
1005 [https://doi.org/10.1016/S0160-4120\(02\)00162-9](https://doi.org/10.1016/S0160-4120(02)00162-9), 2003.
- 1006 Fagerli, H., and Aas, W.: Trends of nitrogen in air and precipitation: model results
1007 and observations at EMEP sites in Europe, 1980-2003, Environ. Pollut. 154,
1008 448–461, <https://doi.org/10.1016/j.envpol.2008.01.024>, 2008.
- 1009 Fenn, M. E., Baron, J. S., Allen, E. B., Rueth, H. M., Nydick, K. R., Geiser, L.,
1010 Bowman, W. D., Sickman, J. O., Meixner, T., Johnson, D. W., and Neitlich, P.:
1011 Ecological Effects of Nitrogen Deposition in the Western United States,
1012 BioScience, 53, 404–420,
1013 [https://doi.org/10.1641/0006-3568\(2003\)053\[0404:EEONDI\]2.0.CO;2](https://doi.org/10.1641/0006-3568(2003)053[0404:EEONDI]2.0.CO;2), 2003.
- 1014 Fowler, D., Smith, R., Muller, J., Cape, J. N., Sutton, M., Erisman, J. W., Fagerli, H.:
1015 2007. Long term trends in sulphur and nitrogen deposition in Europe and the cause
1016 of non-linearities, Water Air Soil Pollut., 7, 41–47,
1017 <https://doi.org/10.1007/s11267-006-9102-x>, 2007.
- 1018 Fowler, D., Coyle, M., Skiba, U., Sutton, M. A., Cape, J. N., Reis, S., Sheppard, L. J.,
1019 Jenkins, A., Grizzetti, B., Galloway, J. N., Vitousek, P., Leach, A., Bouwman, A. F.,
1020 Butterbach-Bahl, K., Dentener, F., Stevenson, D., Amann, M., and Voss, M.: The
1021 global nitrogen cycle in the twenty-first century, Philos. T. R. Soc. B, 368,
1022 20130164, <https://doi.org/10.1098/rstb.2013.0164>, 2013.
- 1023 Fuzzi, S., Baltensperger, U., Carslaw, K., Decesari, S., van Der Gon, H. D., Facchini,
1024 M. C., Fowler, D., Koren, I., Langford, B., Lohmann, U., Nemitz, E., Pandis, S.,
1025 Riipinen, I., Rudich, Y., Schaap, M., Slowik, J. G., Spracklen, D. V., Vignati, E.,
1026 Wild, M., Williams, M. Gilardoni, S.: Particulate matter, air quality and climate:
1027 lessons learned and future needs, Atmos. Chem. Phys., 15, 8217–8299,
1028 <https://doi.org/10.5194/acp-15-8217-2015>, 2015.
- 1029 Galloway, J. N., Townsend, A. R., Erisman, J. W., Bekunda, M., Cai, Z., Freney, J. R.,



- 1030 Martinelli, L. A., Seitzinger, S. P., and Sutton, M. A.: Transformation of the
1031 Nitrogen Cycle: Recent trends, questions, and potential solutions, *Science*, 320,
1032 889–892, <https://doi.org/10.1126/science.1136674>, 2008.
- 1033 Ge, B. Z., Wang, Z. F., Xu, X. B., Wu, J. B., Yu, X. L., and Li, J.: Wet deposition of
1034 acidifying substances in different regions of China and the rest of East Asia:
1035 modeling with updated NAQPMS, *Environ. Pollut.*, 187, 10–21,
1036 <https://doi.org/10.1016/j.envpol.2013.12.014>, 2014.
- 1037 Gilbert, R. O.: Statistical methods for environmental pollution monitoring, John
1038 Wiley & Sons, 1987.
- 1039 Gruber, N. and Galloway, J. N.: An Earth-system perspective of the global nitrogen
1040 cycle, *Nature*, 451, 293–296, <https://doi.org/10.1038/nature06592>, 2008.
- 1041 Gu, B. J., Sutton, M. A., Chang, S. X., Ge, Y., and Jie, C.: Agricultural ammonia
1042 emissions contribute to China’s urban air pollution, *Front. Ecol. Environ.*, 12,
1043 265–266, <https://doi.org/10.1890/14.WB.007>, 2014.
- 1044 Guo, S., Hu, M., Zamora, M. L., Peng, J. F., Shang, D. J., Zheng, J., Du, Z. F., Wu, Z.
1045 J., Shao, M., and Zeng, L. M.: Elucidating severe urban haze formation in China,
1046 *Proc. Natl. Acad. Sci. U.S.A.*, 111, 17373,
1047 <https://doi.org/10.1073/pnas.1419604111>, 2014.
- 1048 Han, X., Zhang, M. G., Skorokhod, A., and Kou, X. X.: Modeling dry deposition of
1049 reactive nitrogen in China with RAMS-CMAQ, *Atmos. Environ.*, 166, 47–61,
1050 <https://doi.org/10.1016/j.atmosenv.2017.07.015>, 2017.
- 1051 He, N. P., Zhu, J. X., and Wang, Q. F.: Uncertainty and perspectives in studies of
1052 atmospheric nitrogen deposition in China: A response to Liu et al. (2015), *Sci.*
1053 *Total Environ.*, 520, 302–304, <https://doi.org/10.1016/j.scitotenv.2015.03.063>,
1054 2015.
- 1055 Huang, P., Zhang, J. B., Xin, X. L., Zhu, A. N., Zhang, C. Z., Ma, D. H., Zhu, Q. G.,
1056 Yang, S., and Wu, S. J.: Proton accumulation accelerated by heavy chemical
1057 nitrogen fertilization and its long-term impact on acidifying rate in a typical arable
1058 soil in the Huang-Huai-Hai Plain, *J. Integr. Agric.* 14, 148–157, 2015.
- 1059 Huang, R. J., Zhang, Y., Bozzetti, C., Ho, K. F., Cao, J. J., Han, Y., Daellenbach, K.



- 1060 R., Slowik, J. G., Platt, S. M., Canonaco, F., Zotter, P., Wolf, R., Pieber, S. M.,
1061 Bruns, E. A., Crippa, M., Ciarelli, G., Piazzalunga, A., Schwikowski, M.,
1062 Abbaszade, G., Schnelle-Kreis, J., Zimmermann, R., An, Z., Szidat, S.,
1063 Baltensperger, U., El Haddad, I., and Prevot, A. S.: High secondary aerosol
1064 contribution to particulate pollution during haze events in China, *Nature*, 514,
1065 218–222, <https://doi.org/10.1038/nature13774>, 2014.
- 1066 Huang, X., Song, Y., Li, M. M., Li, J. F., Huo, Q., Cai, X. H., Zhu, T., Hu, M., and
1067 Zhang, H. S: A high-resolution ammonia emission inventory in China, *Global*
1068 *Biogeochem. Cycles* 26, GB1030, <https://doi.org/10.1029/2011GB004161>, 2012.
- 1069 Ianniello, A., Spataro, F., Esposito, G., Allegrini, I., Rantica, E., Ancora, M. P., Hu,
1070 M., and Zhu, T.: Occurrence of gas phase ammonia in the area of Beijing (China),
1071 *Atmos. Chem. Phys.*, 10, 9487–9503, <https://doi.org/10.5194/acp-10-9487-2010>,
1072 2010.
- 1073 Jia, B., Wang, Y., Yao, Y., and Xie, Y.: A new indicator on the impact of large-scale
1074 circulation on wintertime particulate matter pollution over China, *Atmos. Chem.*
1075 *Phys.*, 15, 11919–11929, <https://doi.org/10.5194/acp-15-11919-2015>, 2015.
- 1076 Jia, Y. L., Yu, G. R., He, N. P., Zhan, X. Y., Fang, H. J., Sheng, W. P., Zuo, Y.,
1077 Zhang, D. Y., and Wang, Q. F.: Spatial and decadal variations in inorganic nitrogen
1078 wet deposition in China induced by human activity, *Sci. Rep.*, 4, 3763,
1079 <https://doi.org/10.1038/srep03763>, 2014.
- 1080 Jia, Y. L.; Yu, G. R.; Gao, Y. N.; He, N. P.; Wang, Q. F.; Jiao, C. C.; and Zuo, Y.:
1081 Global inorganic nitrogen dry deposition inferred from ground and space-based
1082 measurements, *Sci. Rep.*, 6, 19810, <https://doi.org/10.1038/srep19810>, 2016.
- 1083 Kanakidou, M., Myriokefalitakis, S., Daskalakis, N., and Fanourgakis, G.: Past,
1084 present, and future atmospheric nitrogen deposition, *J. Atmos. Sci.*, 73,
1085 160303130433005, <https://doi.org/10.1175/JAS-D-15-0278.s1>, 2016.
- 1086 Karlsson, G. P., Akseleson, C., Hellsten, S., Karlsson, P. E.: Reduced European
1087 emissions of S and N effects on air concentrations, deposition and soil water
1088 chemistry in Swedish forests, *Environ. Pollut.* 159, 3571–3582.
1089 <https://doi.org/10.1016/j.envpol.2011.08.007>, 2011.



- 1090 Khoder, M. I.: Atmospheric conversion of sulfur dioxide to particulate sulfate and
1091 nitrogen dioxide to particulate nitrate and gaseous nitric acid in an urban area,
1092 *Chemosphere*, 49, 675–684, 2002.
- 1093 Krotkov, N. A., McLinden, C. A., Li, C., Lamsal, L. N., Celarier, E. A., Marchenko, S.
1094 V., Swartz, W. H., Bucsela, E. J., Joiner, J., Duncan, B. N., Boersma, K. F.,
1095 Veefkind, J. P., Levelt, P. F., Fioletov, V. E., Dickerson, R. R., He, H., Lu, Z. F.,
1096 and Streets, D. G.: Aura OMI observations of regional SO₂ and NO₂ pollution
1097 changes from 2005 to 2015, *Atmos. Chem. Phys.*, 16, 4605–4629,
1098 <https://doi.org/10.5194/acp-16-4605-2016>, 2016.
- 1099 Kurokawa, J., Ohara, T., Morikawa, T., Hanayama, S., JanssensMaenhout, G., Fukui,
1100 T., Kawashima, K., and Akimoto, H.: Emissions of air pollutants and greenhouse
1101 gases over Asian regions during 2000–2008: Regional Emission inventory in Asia
1102 (REAS) version 2, *Atmos. Chem. Phys.*, 13, 11019–11058,
1103 <https://doi.org/10.5194/acp-13-11019-2013>, 2013.
- 1104 Li, H., Zhang, Q., Zheng, B., Chen, C., Wu, N., Guo, H., Zhang, Y., Zheng, Y., Li, X.,
1105 and He, K.: Nitrate-driven urban haze pollution during summertime over the North
1106 China Plain, *Atmos. Chem. Phys.*, 18, 5293–5306,
1107 <https://doi.org/10.5194/acp-18-5293-2018>, 2018.
- 1108 Li, Y., Niu, S., and Yu, G.: Aggravated phosphorus limitation on biomass production
1109 under increasing nitrogen loading: a meta-analysis, *Global Change Biol.*, 22,
1110 934–943, <https://doi.org/10.1111/gcb.13125>, 2016.
- 1111 Liang, X., Zou, T., Guo, B., Li, S., Zhang, H. Z., Zhang, S. Y., Huang, H., Chen, S.
1112 X.: Assessing Beijing's PM_{2.5} pollution: severity, weather impact, APEC and
1113 winter heating, *Proc. R. Soc. A.*, 471, 20150257,
1114 <https://doi.org/10.1098/rspa.2015.0257>, 2015.
- 1115 Liu, F., Beirle, S., Zhang, Q., van der A, R. J., Zheng, B., Tong, D., and He, K.: NO_x
1116 emission trends over Chinese cities estimated from OMI observations during 2005
1117 to 2015, *Atmos. Chem. Phys.*, 17, 9261–9275,
1118 <https://doi.org/10.5194/acp-17-9261-2017>, 2017.
- 1119 Liu, L., Zhang, X. Y., Zhang, Y., Xu, W., Liu, X. J., Zhang, X. M., Feng, J. L., Chen,



- 1120 X. R., Zhang, Y. H., Lu, X. H., Wang, S. Q., Zhang, W. T., and Zhao, L. M.: Dry
1121 particulate nitrate deposition in China, *Environ. Sci. Technol.*, 51, 5572,
1122 <https://doi.org/10.1021/acs.est.7b00898>, 2017a.
- 1123 Liu, L., Zhang, X., Xu, W., Liu, X., Li, Y., Lu, X., Zhang, Y., Zhang, W.: Temporal
1124 characteristics of atmospheric ammonia and nitrogen dioxide over China based on
1125 emission data, satellite observations and atmospheric transport modeling since 1980,
1126 *Atmos. Chem. Phys.*, 17, 9365–9378, <https://doi.org/10.5194/acp-17-9365-2017>,
1127 2017b.
- 1128 Liu, X.J., Duan, L., Mo, J.M., Du, E.Z., Shen, J.L., Lu, X.K., Zhang, Y., Zhou, X.B.,
1129 He, C.E., Zhang, F.S.: Nitrogen deposition and its ecological impact in China: An
1130 overview, *Environ. Pollut.*, 159, 2251-2264, [https://doi.org/](https://doi.org/10.1016/j.envpol.2010.08.002)
1131 [10.1016/j.envpol.2010.08.002](https://doi.org/10.1016/j.envpol.2010.08.002), 2011.
- 1132 Liu, X. J., Zhang, Y., Han, W. X., Tang, A., Shen, J. L., Cui, Z. L., Vitousek, P.,
1133 Erisman, J. W., Goulding, K., Christie, P., Fangmeier, A., and Zhang, F. S.:
1134 Enhanced nitrogen deposition over China, *Nature*, 494, 459–462,
1135 <https://doi.org/10.1038/nature11917>, 2013.
- 1136 Liu, X. J., Vitousek, P., Chang, Y. H., Zhang, W. F., Matson, P., and Zhang, F. S.:
1137 Evidence for a historic change occurring in China, *Environ. Sci. Technol.*, 50,
1138 505–506, <https://doi.org/10.1021/acs.est.5b05972>, 2016.
- 1139 Lu, C. Q. and Tian, H. Q.: Spatial and temporal patterns of nitrogen deposition in
1140 China: Synthesis of observational data, *J. Geophys. Res.*, 112, D22S05,
1141 <https://doi.org/10.1029/2006JD007990>, 2007.
- 1142 Lu, C. Q. and Tian, H. Q.: Half-century nitrogen deposition increase across China: A
1143 gridded time-series data set for regional environmental assessments, *Atmos.*
1144 *Environ.*, 97, 68–74, <https://doi.org/10.1016/j.atmosenv.2014.07.061>, 2014.
- 1145 Marchetto, A., Rogora, M., and Arisci, S.: Trend analysis of atmospheric deposition
1146 data: A comparison of statistical approaches, *Atmos. Environ.*, 64, 95–102, 2013.
- 1147 Meng, Z. Y., Xu, X. B., Wang, T., Zhang, X. Y., Yu, X. L., Wang, S. F., Lin, W. L.,
1148 Chen, Y. Z., Jiang, Y. A., and An, X. Q.: Ambient sulfur dioxide, nitrogen dioxide,
1149 and ammonia at ten background and rural sites in China during 2007-2008, *Atmos.*



- 1150 Environ., 44, 2625–2631.
- 1151 Meng, Z. Y., Xu, X. B., Lin, W. L., Ge, B. Z., Xie, Y. L., Song, B., Jia, S. H., Zhang,
1152 R., Peng, W., Wang, Y., Cheng, H. B., Yang, W., and Zhao, H.: Role of ambient
1153 ammonia in particulate ammonium formation at a rural site in the North China
1154 Plain, Atmos. Chem. Phys., 18, 167–184, <https://doi.org/10.5194/acp-18-167-2018>,
1155 2018.
- 1156 MEPC (Ministry of Environmental Protection of the People's Republic of China):
1157 Report on Environmental Quality in China, 2010. Available online at:
1158 http://jcs.mep.gov.cn/hjzl/zkgb/2010zkgb/201106/t20110602_211579.htm, 2011.
- 1159 Miyazaki, K., Eskes, H., Sudo, K., Boersma, K. F., Bowman, K., and Kanaya, Y.:
1160 Decadal changes in global surface NO_x emissions from multi-constituent satellite
1161 data assimilation, Atmos. Chem. Phys., 17, 807–837,
1162 <https://doi.org/10.5194/acp-17-807-2017>, 2017.
- 1163 Pan, Y. P., Wang, Y. S., Tang, G. Q., and Wu, D.: Wet and dry deposition of
1164 atmospheric nitrogen at ten sites in Northern China, Atmos. Chem. Phys., 12,
1165 6515–6535, <https://doi.org/10.5194/acp-12-6515-2012>, 2012.
- 1166 Pan, Y. P., Wang, Y. S., Zhang, J. K., Liu, Z. R., Wang, L. L., Tian, S. L., Tang, G.
1167 Q., Gao, W. K., Ji, D. S., and Song, T.: Redefining the importance of nitrate during
1168 haze pollution to help optimize an emission control strategy, Atmos. Environ., 141,
1169 197–202, <http://dx.doi.org/10.1016/j.atmosenv.2016.06.035>, 2016.
- 1170 Pinder, R. W., Walker, J. T., Bash, J. O., Cady-Pereira, K. E., Henze, D. K., Luo, M.
1171 Z., Osterman, G. B., and Shephard, M. W.: Quantifying spatial and seasonal
1172 variability in atmospheric ammonia with in situ and space-based observations,
1173 Geophys. Res. Lett., 38, L04802, <https://doi.org/10.1029/2010GL046146>, 2011.
- 1174 Russell, A. R., Valin, L. C., and Cohen, R. C.: Trends in OMI NO₂ observations over
1175 the United States: effects of emission control technology and the economic
1176 recession, Atmos. Chem. Phys., 12, 12197–12209,
1177 <https://doi.org/10.5194/acp-12-12197-2012>, 2012.
- 1178 Salmi, T., Maatta, A., Anttila, P., Ruoho-Airola, T., and Amnell, T.: Detecting trends
1179 of annual values of atmospheric pollutants by the Mann–Kendall test and Sen's



- 1180 slope estimates—the Excel template application MAKESENS. Publications on Air
1181 Quality No. 31, Finnish Meteorological Institute, Helsinki, Finland, 2002.
- 1182 Seinfeld, J. H. and Pandis, S. N.: Atmospheric chemistry and physics: from air
1183 pollution to climate change, 2nd Edn., Wiley Interscience, New Jersey, 2006.
- 1184 She, W.: Hu Huanyong: father of China's population geography, China Popul. Today
1185 15, 1–20, 1998.
- 1186 Souri, A. H., Choi, Y., Jeon, W., Woo, J.-H., Zhang, Q., and Kurokawa, J.-i.: Remote
1187 sensing evidence of decadal changes in major tropospheric ozone precursors over
1188 East Asia, *J. Geophys. Res.*, 122, 2474–2492,
1189 <https://doi.org/10.1002/2016JD025663>, 2017.
- 1190 Tang, Y. S., Simmons, I., van Dijk, N., Di Marco, C., Nemitz, E., Dammgen, U.,
1191 Gilke, K., Djuricic, V., Vidic, S., and Gliha, Z.: European scale application of
1192 atmospheric reactive nitrogen measurements in a low-cost approach to infer dry
1193 deposition fluxes, *Agr. Ecosyst. Environ.*, 133, 183–195, <https://doi.org/10.1016/j.agee.2009.04.027>, 2009.
- 1195 Theil, H.: A Rank-Invariant Method of Linear and Polynomial Regression Analysis,
1196 in: Henri Theil's Contributions to Economics and Econometrics, edited by: Raj, B.
1197 and Koerts, J., *Advanced Studies in Theoretical and Applied Econometrics*,
1198 Springer Netherlands, 345–381, 1992.
- 1199 Tian, S. L., Pan, Y. P., Liu, Z. R., Wen, T. X., and Wang, Y. S.: Size-resolved aerosol
1200 chemical analysis of extreme haze pollution events during early 2013 in urban
1201 Beijing, China, *J. Hazard. Mater.*, 279, 452–460, <https://doi.org/10.1016/j.jhazmat.2014.07.023>, 2014.
- 1203 Van Damme, M., Clarisse, L., Dammers, E., Liu, X., Nowak, J. B., Clerbaux, C.,
1204 Flechard, C. R., Galycaux, C., Xu, W., and Neuman, J. A.: Towards validation of
1205 ammonia (NH₃) measurements from the IASI satellite, *Atmos. Meas. Tech.*, 8,
1206 1575–1591, <https://doi.org/10.5194/amt-8-1575-2015>, 2015.
- 1207 van der A, R. J., Mijling, B., Ding, J., Koukouli, M. E., Liu, F., Li, Q., Mao, H., and
1208 Theys, N.: Cleaning up the air: effectiveness of air quality policy for SO₂ and NO_x
1209 emissions in China, *Atmos. Chem. Phys.*, 17, 1775–1789,



- 1210 <https://doi.org/10.5194/acp-17-1775-2017>, 2017.
- 1211 Vet, R., Artz, R. S., Carou, S., Shaw, M., Ro, C.-U., Aas, W., Baker, A., Bowersox, V.
1212 C., Dentener, F., Galy-Lacaux, C., Hou, A., Pienaar, J. J., Gillett, R., Forti, M. C.,
1213 Gromov, S., Hara, H., Khodzher, T., Mahowald, N. M., Nickovic, S., Rao, P. S. P.,
1214 and Reid, N. W.: A global assessment of precipitation chemistry and deposition of
1215 sulfur, nitrogen, sea salt, base cations, organic acids, acidity and pH, and
1216 phosphorus, *Atmos. Environ.*, 93, 3–100, <https://doi.org/10.1016/j.atmosenv.2013.10.060>, 2014.
- 1218 Walker, J. T., Whitall, D. R., Robarge, W., and Paerl, H. W.: Ambient ammonia and
1219 ammonium aerosol across a region of variable ammonia emission density, *Atmos.*
1220 *Environ.*, 38, 1235–1246, 2004.
- 1221 Wang, G. H., Zhang, R. Y., Gomez, M. E., Yang, L. X., Zamora, M. L., Hu, M., Lin,
1222 Y., Peng J. F., Guo, S., Meng, J. J., Li, J. J., Cheng, C. L., Hu, T. F., Ren, Y. Q.,
1223 Wang, Y. S., Gao, J., Cao, J. J., An, Z. S., Zhou, W. J., Li, G. H., Wang, J. Y., Tian,
1224 P. F., Marrero-Ortiz, W., Secret J., Du, Z. F., Zheng, J., Shang, D. J., Zeng, L. M.,
1225 Shao, M., Wang, W. G., Huang, Y., Wang, Y., Zhu, Y. J., Li, Y. X., Hu, J. X., Pan,
1226 B. W., Cai, L., Cheng, Y. T., Ji, Y. M., Zhang, F., Rosenfeld, D., Liss, P. S., Duce,
1227 R. A., Kolb, C. E., and Molina, M. J.: Persistent sulfate formation from London
1228 Fog to Chinese haze, *Proc. Natl. Acad. Sci. U.S.A.*, 113, 13630, <https://doi.org/10.1073/pnas.1616540113>, 2016.
- 1230 Wang, S. X., Xing, J., Jang, C. R., Zhu, Y., Fu, J. S., and Hao, J. M.: Impact
1231 assessment of ammonia emissions on inorganic aerosols in East China using
1232 response surface modeling technique, *Environ. Sci. Technol.*, 45, 9293–9300,
1233 <https://doi.org/10.1021/es2022347>, 2011.
- 1234 Wen, L., Chen, J. M., Yang, L. X., Wang, X. F., Xu, C. H., Sui, X., Yao, L., Zhu, Y.
1235 H., Zhang, J. M., Zhu, T., and Wang, W. X.: Enhanced formation of fine particulate
1236 nitrate at a rural site on the North China Plain in summer: The important roles of
1237 ammonia and ozone, *Atmos. Environ.*, 101, 294–302,
1238 <http://dx.doi.org/10.1016/j.atmosenv.2014.11.037>, 2015.
- 1239 Wesely, M. L.: Parameterization of surface resistances to gaseous dry deposition in



- 1240 regional-scale numerical-models, *Atmos. Environ.*, 23, 1293–1304, 1989.
- 1241 Whitburn, S., Van Damme, M., Clarisse, L., Bauduin, S., Heald, C. L., Hadji-Lazaro,
1242 J., Hurtmans, D., Zondlo, M. A., Clerbaux, C., and Coheur, P. F.: A flexible and
1243 robust neural network IASINH3 retrieval algorithm, *J. Geophys. Res.-Atmos.*, 121,
1244 6581–6599, <https://doi.org/10.1002/2016JD024828>, 2016.
- 1245 Xia, Y. M., Zhao, Y., and Nielsen, C. P.: Benefits of China's efforts in gaseous
1246 pollutant control indicated by the bottom-up emissions and satellite observations
1247 2000–2014, *Atmos. Environ.*, 136, 43–53, <https://doi.org/10.1016/j.atmosenv.2016.04.013>, 2016.
- 1249 Xu, W., Luo, X.S., Pan, Y.P., Zhang, L., Tang, A.H., Shen, J.L., Zhang, Y., Li, K.H.,
1250 Wu, Q.H., Yang, D.W., Zhang, Y.Y., Xue, J., Li, W.Q., Li, Q.Q., Tang, L., Lu,
1251 S.H., Liang, T., Tong, Y.A., Liu, P., Zhang, Q., Xiong, Z.Q., Shi, X.J., Wu, L.H.,
1252 Shi, W.Q., Tian, K., Zhong, X.H., Shi, K., Tang, Q.Y., Zhang, L.J., Huang, J.L., He,
1253 C.E., Kuang, F.H., Zhu, B., Liu, H., Jin, X., Xin, Y.J., Shi, X.K., Du, E.Z., Dore,
1254 A.J., Tang, S., Collett, J.L., Goulding, K., Sun, Y.X., Ren, J., Zhang, F.S., and Liu,
1255 X.J.: Quantifying atmospheric nitrogen deposition through a nationwide monitoring
1256 network across China. *Atmos. Chem. Phys.*, 15, 12345–12360, <https://doi.org/10.5194/acp-15-12345-2015>, 2015.
- 1258 Xu, W., Wu, Q. H., Liu, X. J., Tang, A. H., Dore, A. J., and Heal, M. R.:
1259 Characteristics of ammonia, acid gases, and PM_{2.5} for three typical land-use types
1260 in the North China Plain, *Environ. Sci. Pollut. Res.*, 23, 1158–1172, <https://doi.org/10.1007/s11356-015-5648-3>, 2016.
- 1262 Xu, W., Song, W., Zhang, Y., Liu, X., Zhang, L., Zhao, Y., Liu, D., Tang, A., Yang,
1263 D., Wang, D., Wen, Z., Pan, Y., Fowler, D., Collett Jr., J. L., Erisman, J. W.,
1264 Goulding, K., Li, Y., and Zhang, F.: Air quality improvement in a megacity:
1265 implications from 2015 Beijing Parade Blue pollution control actions, *Atmos.*
1266 *Chem. Phys.*, 17, 31–46, <https://doi.org/10.5194/acp-17-31-2017>, 2017.
- 1267 Xu, W., Zhao, Y. H., Liu, X. J., Dore, A. J., Zhang, L., Liu, L., and Cheng, M.:
1268 Atmospheric nitrogen deposition in the Yangtze River basin: Spatial pattern and
1269 source attribution, *Environ. Pollut.*, 232, 546–555,



- 1270 <https://doi.org/10.1016/j.envpol.2017.09.086>, 2018.
- 1271 Yang, F., Tan, J., Zhao, Q., Du, Z., He, K., Ma, Y., Duan, F., Chen, G., and Zhao, Q.:
1272 Characteristics of PM_{2.5} speciation in representative megacities and across China,
1273 Atmos. Chem. Phys., 11, 5207–5219, <https://doi.org/10.5194/acp-11-5207-2011>,
1274 2011.
- 1275 Yang, Y. H., Li, P., He, H. L., Zhao, X., Datta, A., Ma, W. H., Zhang, Y., Liu, X. J.,
1276 Han, W. X., Wilson, M. C., and Fang, J. Y.: Long-term changes in soil pH across
1277 major forest ecosystems in China, Geophys. Res. Lett., 42,
1278 <https://doi.org/10.1002/2014GL062575>, 2015.
- 1279 Zhao, Y., Nielsen, C. P., Lei, Y., McElroy, M. B., and Hao, J.: Quantifying the
1280 uncertainties of a bottom-up emission inventory of anthropogenic atmospheric
1281 pollutants in China, Atmos. Chem. Phys., 11, 2295–2308,
1282 <https://doi.org/10.5194/acp-11-2295-2011>, 2011.
- 1283 Zhang, L., Chen, Y. F., Zhao, Y. H., Henze, D. K., Zhu, L. Y., Song, Y., Paulot, F.,
1284 Liu, X. J., Pan, Y. P., and Huang, B. X.: Agricultural ammonia emissions in China:
1285 reconciling bottom-up and top-down estimates, Atmos. Chem. Phys., 18, 339–355,
1286 <https://doi.org/10.5194/acp-18-339-2018>, 2018.
- 1287 Zhang, L. M., Gong, S. L., Padro, J., and Barrie, L.: A size-segregated particle dry
1288 deposition scheme for an atmospheric aerosol module, Atmos. Environ., 35,
1289 549–560, [https://doi.org/10.1016/s1352-2310\(00\)00326-5](https://doi.org/10.1016/s1352-2310(00)00326-5), 2001.
- 1290 Zhang, Q., Duan, F. K., He, K. B., Ma, Y. L., Li, H. Y., Kimoto, T., Zheng, A. H.:
1291 Organic nitrogen in PM_{2.5} in Beijing, Front. Env. Sci. Eng., 9, 1004–1014,
1292 <https://doi.org/10.1007/s11783-015-0799-5>, 2015.
- 1293 Zhang, X. M., Wu, Y. Y., Liu, X. J., Reis, S., Jin, J. X., Dragosits, U., Damme, Van
1294 M., Clarisse, L., Whitburn, S., and Coheur, P. F.: Ammonia emissions may be
1295 substantially underestimated in China, Environ. Sci. Technol., 51, 12089–12096,
1296 <https://doi.org/10.1021/acs.est.7b02171>, 2017.
- 1297 Zhao, Y., Zhang, L., Pan, Y., Wang, Y., Paulot, F., and Henze, D. K.: Atmospheric
1298 nitrogen deposition to the northwestern Pacific: seasonal variation and source
1299 attribution, Atmos. Chem. Phys., 15, 10905–10924,



- 1300 <https://doi.org/10.5194/acp-15-10905-2015>, 2015.
- 1301 Zhao, Y., Zhang, L., Chen, Y. F., Liu, X. J., Xu, W., Pan, Y. P., and Duan, L.:
- 1302 Atmospheric nitrogen deposition to China: a model analysis on nitrogen budget and
- 1303 critical load exceedance, Atmos. Environ., 153, 32–40,
- 1304 <https://doi.org/10.1016/j.atmosenv.2017.01.018>, 2017.
- 1305 Zhu, J. X., He, N. P., Wang, Q. F., Yan, G. F., Wen, D., Yu, G. R., and Jia, Y. L.: The
- 1306 composition, spatial patterns, and influencing factors of atmospheric wet nitrogen
- 1307 deposition in Chinese terrestrial ecosystems, Sci. Total Environ., 511, 777–785,
- 1308 <https://doi.org/10.1016/j.scitotenv.2014.12.038>, 2015.
- 1309